

# RES TERRAE

Publications of the Department of Geosciences University of Oulu  
Oulun yliopiston geotieteiden laitoksen julkaisuja

Ser. A, No. 31  
2010

Pekka Tuisku and Jüri Nemliher  
Editors

Proceedings of the 5<sup>th</sup> Annual Meeting of Nordic Mineralogical Network, Tallinn,  
14<sup>th</sup>-18<sup>th</sup> June 2010





**Pekka Tuisku and Jüri Nemliher**

**Editors**

**Proceedings of the 5<sup>th</sup> Annual Meeting of Nordic Mineralogical Network,  
Tallinn, 14<sup>th</sup>-18<sup>th</sup> June 2010**

**Res Terrae, Ser. A, No. 31, OULU, 2010**



**RES TERRAE** - Publications of the Department of Geosciences,  
University of Oulu, Oulun yliopiston geotieteiden laitoksen julkaisuja

**Ser. A, Contributions**

**ISSN 0358-2477**

**Ser. B, Raportteja - Reports**

**ISSN 0358-2485**

**Ser. C, Opetusjulkaisuja - Teaching material**

**ISSN 0358-2493**

**Editorial board - Toimituskunta:**

**Dr. Pekka Tuisku, Päätoimittaja - Editor-in-Chief**

**Prof. Vesa Peuraniemi**

**Dr. Aulis Kärki, Toimitussihteeri - Sub-Editor**

**Julkaisu ja levitys - Published and distributed by:**

**Oulun yliopisto, geologian osasto - University of Oulu, Department of  
Geology, P.O. Box 3000, 90014 University of Oulu, Finland**

**Telephone: 08-5531430, International tel: +358-8-5531430**

**Telefax: 08-5531484, International fax: +358-8-5531484**

**E-mail: pekka.tuisku@oulu.fi**

**www: <http://cc.oulu.fi/~resterr/>**

Cover Figure: *Recent secondary dolomite crystals growing on the Cliff of Pakri , Cape Paldiski (Photo P.Tuisku)*

## Contents

<b>Mineralogy of encrustations from the recently and presently active Icelandic volcanoes</b> Tonči Balić-Žunić, Sveinn Peter Jakobsson and Anna Garavelli	4
<b>Thermal expansion of CaIrO<sub>3</sub></b> Anna Katerinopoulou, Tonci Balic-Zunic, Hannes Krüger, Volker Kahlenberg and Reidar Trønnes	8
<b>Diagenetic chlorite and its relation to reservoir properties in Tyr Member sandstone, Siri Canyon, Danish North Sea</b> A. M. Kazerouni, H. Friis and J. P. V. Hansen	12
<b>Active silica sources in the Sele formation and quartz cementation in mudstone - Examples from the Siri Canyon, Danish North Sea</b> A. M. Kazerouni, H. Friis and J. B. Svendsen	19
<b>Partial replacement of alite by Klein's compound: An approach to reduce cement related CO<sub>2</sub> emissions? A laboratory study</b> Maria Rosenberger Rasch, Hans Dieter Zimmermann, Duncan Herfort and Lise Frank Kirkegaard	24
<b>PGM and PGE alloy nuggets- and Au-nuggets from alluvial deposits in Finnish Lapland</b> Ragnar Törnroos and Kari Kojonen	28
<b>Heavy minerals from gold sluicings in Lapland Gold Rush areas, and their bearing on the origin of gold bearing tills</b> Pekka Tuisku	33
<b>Origin of corundum in Lapland</b> Pekka Tuisku and Kimmo Lahtinen	38
<b>Geochemistry and P–T conditions of magnetite quartzites from Jõhvi Zone, NE Estonia</b> Margus Voolma, Alvar Soesoo and Sigrid Hade	42
<b>Optical Mineralogy – An Anachronism?</b> Hans Dieter Zimmermann	47
<b>Teaching Optical Mineralogy: Practical Suggestions</b> Hans Dieter Zimmermann	52
<b>Experimental study on carbon dioxide contents in basanitic and leucititic melts</b> Hans Dieter Zimmermann and John R. Holloway	64

## **Mineralogy of encrustations from the recently and presently active Icelandic volcanoes**

Tonči Balić-Žunić 1), Sveinn Peter Jakobsson 2) and Anna Garavelli 3)

1) *Natural History Museum, University of Copenhagen, Denmark*

2) *Icelandic Institute of Natural History*

3) *Dipartimento Geomineralogico, Università di Bari, Italy*

Fumarolic minerals are formed either as sublimates by a direct condensation from gases or through reaction of gases with the solid rock. Mineralogy of fumaroles is distinct, very rich and often varies significantly between volcanoes or during the history of the same volcano. This often remains unnoticed, due to the short life of fumarolic minerals which are exposed to weathering and very sensitive to physical and chemical erosion. Their identification is also very difficult due to complex mixtures and minute sizes of the crystals.

Fumarolic minerals are interesting as natural occurrences of rare compounds with specific properties, deposits of economic importance (e.g. of sulphur, halogenides, rare metals), as records and sensors of the volcanic activity and finally as the sources of pollution.

Our investigations on three Icelandic volcanoes suggest that a significant part of the sulphuric gases and fluorine emitted after the explosive eruptions reacts at or close to surface to form minerals. Through this process, the large amount of these elements is released to the environment as dust particles or in water solution through subsequent fast erosion. The composition of the fumarolic minerals varies systematically from sulfate-rich on Surtsey to fluoride-rich on Hekla. The composition on Eldfell, which lies between them, is a transitional one with both components equally represented. This is most probably due to differences in magma compositions, as testified by previous analyses of lavas and our investigation of stable sulphur isotopes which for all three localities have typical values for volcanic sources.

Hekla (1491 m) is one of the most active volcanoes in Iceland, with more than 18 eruptions recorded during historical time. The 1991 Hekla eruption lasted for two months. A considerable amount of volcanic gases and vapor was released during the eruption. Pollution of groundwater and rivers around the volcano by e. g. fluorine, was observed already a few days after the onset of the eruption.

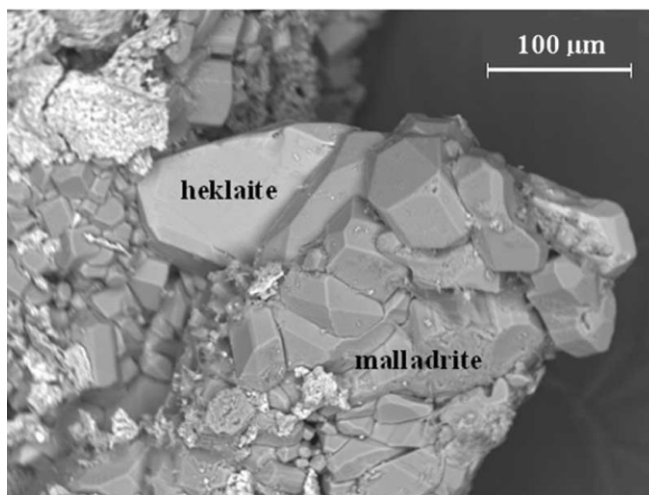


Figure 1. SEM image of the new mineral heklaite in association with malladrite.

The study of the fumarolic encrustations discovered altogether 36 different minerals, of which 17 are new mineral species (Jakobsson et al. 2008), presently under detailed study by our research team. The most common among the minerals are opal (amorphous silica), hematite (iron oxide) and four fluorides, two of them already known as minerals (ralstonite and malladrite) and two new ones: recently described heklaite with composition  $\text{KNaSiF}_6$  (Garavelli et al. 2010), and a still not named mineral with the composition  $\text{CaAlF}_5$ .



Figure 2. Thenardite (white cover on the lava blocks in the foreground at Fimmvörduhals, Eyjafjallajökull on April 7, 2010.

Eruption on Eyjafjallajökul in March/April 2010 sent a large amount of volcanic ash in the atmosphere, disturbing the air traffic over the large part of Europe and filling the world news. Already during the eruption we were collecting the samples on the fresh fumaroles and could preliminary

determine the sulphate thenardite plus two fluorides: ralstonite and an ammonium-iron fluoride which is one of the new minerals recorded earlier on Hekla.

Surtsey eruption which lasted from 1963 to 1967 is one of the most spectacular in the modern history. It was a submarine eruption which formed a new island which now is a protected natural reserve. The island became a scientific laboratory with a specific purpose to investigate the whole life cycle of a volcanic island from its birth.

Investigation of fumarolic encrustations which could be collected from various sites on the surface, vents, fissures and caves, revealed over 30 different minerals of which six appear to be new mineral species observed only at this place (Jakobsson et al. 2008). Although the fluoride ralstonite and oxide hematite appear at lava surfaces, the mineralogy is dominated by sulphates which form the main mass on various cave walls. The minerals here were formed both from volcanic gases and from the steaming sea water, and the presence of halite (sodium chloride) is also characteristic for Surtsey.

The eruption of Eldfell on the Heimaey island in 1973 was the most dramatic one in the history of Iceland. The volcano started its activity unexpectedly on the very outskirts of the town which is the most important fishing harbour of Iceland. In few days the whole population was evacuated from the island and a large action was started in spraying the sea water on the approaching lava which threatened to close the entrance to this important harbour. The harbour was saved and the life on the island reestablished after the volcano ceased to erupt. However, the fumaroles on the top of the crater are still active and our expedition in 2009 collected freshly forming fumarolic minerals and measured the temperatures in fumaroles well in excess of 300°C.

We could determine around 30 different minerals in fumaroles. About 10 are new minerals, half of them also observed on Hekla (Jakobsson et al. 2008). One of the minerals has been recently fully described and named eldfellite. It is a sulphate with the composition  $\text{NaFe}(\text{SO}_4)_2$  (Balic-Zunic et al. 2009). Fluorides on Eldfell, among which ralstonite (in mixture with hematite) is the dominating species, are mostly connected to the hotter fumaroles, whereas calcium sulphates anhydrite and gypsum dominate among sulphates at lower-temperated ones. Leaching of lava by gases can be observed on several places where the rocks have been completely turned to opal.



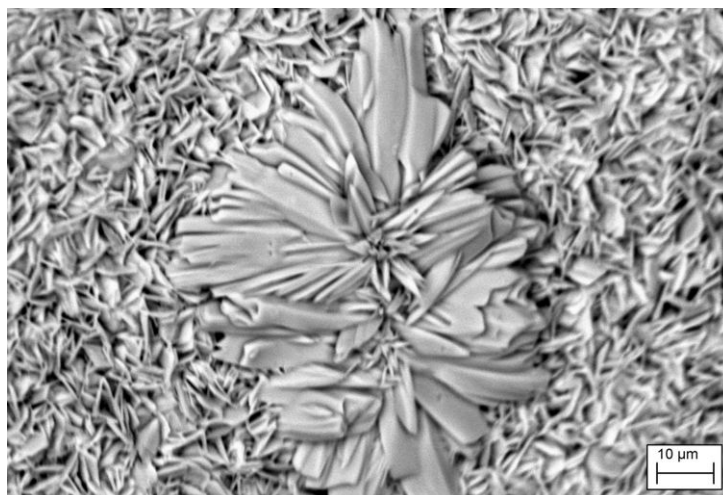


Figure 3. SEM image of eldfellite rosette on the background of platy tamarugite crystals.

Material from fumaroles is a mixture of many minerals which form fine crystalline aggregates. Specialized methods for the mineral identification and characterization are needed to analyze this type of material. We are applying the Powder X-Ray Diffraction for the identification of mineral species, the Scanning Electron Microscopy for the investigation of morphology, and the Energy Dispersive X-Ray Spectroscopy coupled to the same instrument for the determination of the chemical composition.

## References

Balić-Žunić, T., Garavelli, A., Acquafredda, P., Leonardsen, E. and Jakobsson, S.P. 2009. Eldfellite,  $\text{NaFe}(\text{SO}_4)_2$ , a new fumarolic mineral from Eldfell volcano, Iceland. *Mineralogical Magazine*, **73**, 51-57.

Garavelli, A., Balić-Žunić, T., Mitolo, D., Acquafredda, P., Leonadsen, E. and Jakobsson, S.P. 2010. Heklaite,  $\text{KNaSiF}_6$ , a new fumarolic mineral from Hekla volcano, Iceland. *Mineralogical Magazine*, **74**, 147-157.

Jakobsson, S.P., Leonardsen, E., Balic-Zunic, T. and Jónsson, S.S. 2008. Encrustations from three recent volcanic eruptions in Iceland: The 1963-1967 Surtsey, the 1973 Eldfell and the 1991 Hekla eruptions. *Fjölrit Náttúrufræðistofnunar*, **52**, 65 p.

## **Thermal expansion of CaIrO<sub>3</sub>**

Anna Katerinopoulou<sup>1</sup>, Tonci Balic-Zunic<sup>1</sup>, Hannes Krüger<sup>2</sup>, Volker Kahlenberg<sup>2</sup>, Reidar Trønnes<sup>3</sup>

1) *Department of Geography and Geology, University of Copenhagen, Denmark (email: aka@geo.ku.dk)*

2) *Institute of Mineralogy and Petrography, University of Innsbruck, Austria*

3) *Department of Geology and Mineral Resources Engineering, NTNU Trondheim, Norway*

Deep Earth dynamics are greatly affected by the MgSiO<sub>3</sub> perovskite (pv) to post-perovskite (ppv) transition. Perovskite is believed to be the most abundant mineral in the lower mantle. The transition conditions correspond to the D"-zone, which has long been an enigmatic region in the boundary between the Earth's mantle and core. The thermodynamic properties of the transition would give important constrains on the phase stability relations. However, such a study can only be performed on an analogue material, because the perovskite phase of MgSiO<sub>3</sub> is not stable in ambient conditions. CaIrO<sub>3</sub> is the only known material where both pv and ppv phases are quenchable at 1 atm. It is stable at 1 atm as ppv (Cmcm) and also crystallizes as metastable orthorhombic pv phase (Pbnm) (Stølen and Trønnes, 2007).

In-situ single-crystal X-ray diffraction experiments were carried out with a STOE IPDS-II two-circle diffractometer equipped with an image plate detector. Heating was achieved by a hot N<sub>2</sub> gas flow from a Heatstream device (STOE and Cie GmbH). The heater was operated at a constant flow of 0.8 l/min N<sub>2</sub>, regulated by a mass flow controller. The crystals under investigation were embedded in SiO<sub>2</sub> glass capillaries, diffraction experiments were performed at different temperatures from 372.15 K up to 1072.15 K in steps of 100 K for perovskite and 200 K for post-perovskite respectively.

At atmospheric pressure the stable form of CaIrO<sub>3</sub> is the orthorhombic post-perovskite (Cmcm). The orthorhombic CaIrO<sub>3</sub> perovskite (Pbnm) forms as a metastable phase, but during heating there was no indication of a phase transition. The reflections remained sharp, they were all indexed and the e.s.d's of the lattice parameters at elevated temperatures are comparable to the ones at room-temperature.

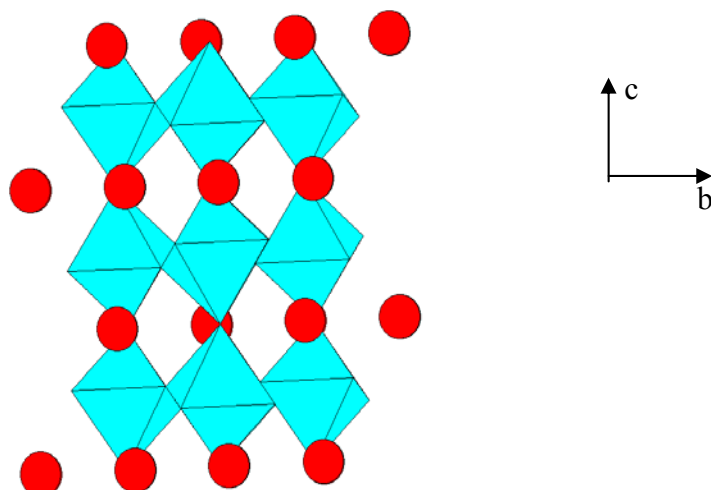


Figure 1. View of the post-perovskite (Cmcm) structure along the a axis. Red: Ca-atoms, Blue: Ir-O octahedra

Post-perovskite type  $\text{CaIrO}_3$  consists of single layers of  $\text{IrO}_6$  octahedra normal to the b-axis (Fig 1). The octahedra share edges along the a-axis and corners along the c-axis, while calcium occupies sites between these layers. In the case of the post-perovskite structure, an anisotropic linear expansion is observed (Fig 2). The b-axis, which is normal to the edge-linked octahedra, shows the largest expansion. Data can be fitted with a second-order Grüneisen approximation curve (Lindsay-Scott et al., 2007).

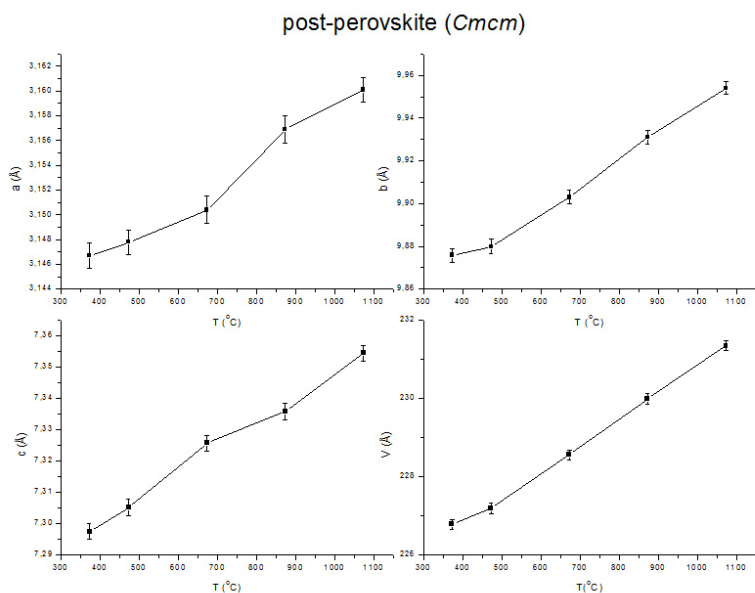


Figure 2. The variation with temperature of the lattice of  $\text{CaIrO}_3$  postperovskite. The data are in agreement with previous investigations in powder samples by Lindsay-Scott et al., 2007

The  $Pbnm$  perovskite is a more open and flexible crystal structure, where the octahedra are corner linked forming a 3-dimensional frame (Fig 3). Between them the Ca-atoms are situated. The octahedra along the  $c$ -axes are rotated relative to the post-perovskite structure, whereas along the other directions they are rotated in an opposite sense by the same rotation angle.

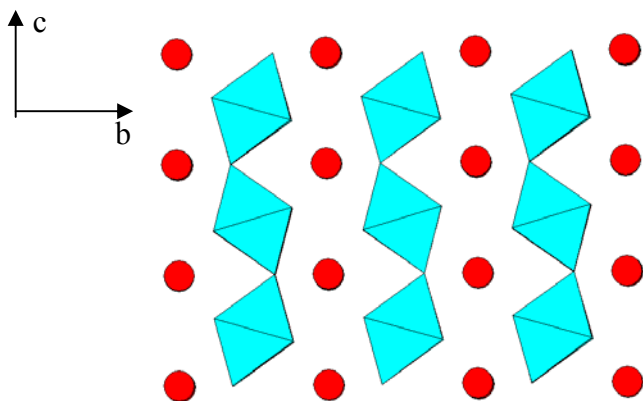


Figure 3. View of the perovskite ( $Pbnm$ ) structure along the  $a$  axis. Red: Ca-atoms, Blue: Ir-O octahedra

An even larger anisotropy is observed in this case, the expansion curve of the  $b$ -axis has a negative slope (Fig 4). The  $a$ - and  $c$ - axes expand with temperature while the  $b$ -axis contracts. There some deviation from linear expansion appears around 972.15 K.

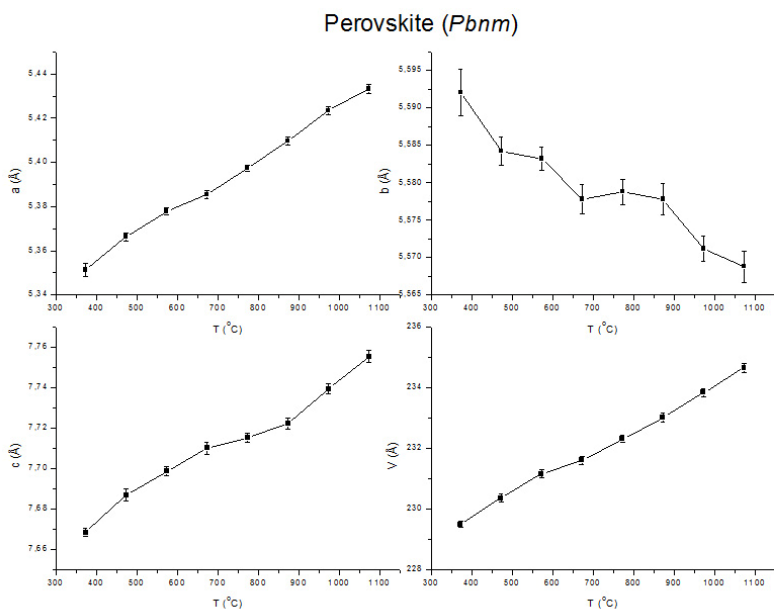


Figure 4. The variation with temperature of the lattice of  $CaIrO_3$  perovskite. Note the contraction of  $b$ -axis with increasing temperature

Although the post-perovskite phase is known to undergo a transition to perovskite at high temperatures, no sign of a space group change was observed. The contraction of b-axis in the perovskite-type structure is of particular interest. It suggests that the  $[\text{IrO}_6]$  octahedra in the structure rotate in the sense that diminishes the discrepancy to the ideal cubic archetype.

## References

Lindsay-Scott, A. Wood, I.G. and Dobson, D.P. 2007. Thermal expansion of  $\text{CaIrO}_3$  determined by X-ray powder diffraction. *Phys. of the earth and planet. inter.*, Number 162, 140p.

Stølen, S. and Trønnes, R.G. 2007. The perovskite to post-perovskite transition in  $\text{CaIrO}_3$ : Clapeyron slope and changes in bulk and shear moduli by density functional theory. *Phys. of the earth and planet. inter.*, Number 164, 50 p.

## **Diagenetic chlorite and its relation to reservoir properties in Tyr Member sandstone, Siri Canyon, Danish North Sea**

A. M. Kazerouni<sup>1</sup>, H. Friis<sup>1</sup>, J. P. V. Hansen<sup>2</sup>

1) *Department of Earth Sciences, Aarhus University*

2) *Noreco Oil Denmark*

### **Abstract**

To evaluate the possible changes in petrology within the reservoir sand and across the oil water contact in Rau-1A, Siri Canyon Danish North Sea, 32 samples were selected and studied mainly by electron microscope and XRD.

The major diagenetic phases in the well are micro quartz, large syntaxial quartz overgrowths, calcite, chlorite, and also minor amount of diagenetic K-feldspar. The investigated materials were core samples of Palaeocene sands referred to the Tyr Member from the well Rau-1A. Chlorite was formed as pervasive grain-coating cement, but much porosity was still present. In the oil-zone and deeper, porous samples were later cemented by macro quartz, with larger amounts in the water zone. Above the oil zone of the reservoir, the sandstone is tightly cemented by chlorite.

Chlorite can be recognized in SEM as a platy or bladed precipitate, which is mostly rich in iron. Chlorite is present in most samples, although only in traceable amounts in the samples, which are dominated by microquartz cement.

There seem to be two chlorite phases: The first phase occurs as rosettes in a grain coating growth pattern. It is partially intergrown with microquartz or forms a dense mixture of small chlorite rosettes and scattered microquartz.

Pore-lining chlorite is partially post-compactional and grows into fractures in glauconite grains. Pore lining chlorite is formed prior to macroquartz and post-compactional calcite; whereas early calcite cemented samples did not evolve chlorite.

The general impression is, however, that chlorite cement is more abundant and better developed in the lower parts of reservoir units, whereas it may be scarce and poorly developed in upper parts,

especially within the oil zone. Below the oil-water contact, the growth of chlorite may have continued for a longer period, resulting in more dense coatings, which are very destructive for permeability.

## **Introduction**

The aim of this study is to determine the evolutionary history of the chlorite cement and to relate it to the development of reservoir properties, especially the formation of an intra-reservoir seal of diagenetic chlorite. Investigations within the reservoir sand and across the oil-water contact may lead to an improved understanding of the diagenetic history, preservation of porosity and permeability and interaction between diagenesis and hydrocarbon. On basis of XRD data it is possible to demonstrate a slight shift of actual peak position in overlapping peaks of chlorite in the studied samples. This variation indicates two facies of chlorite in different time. On basis of the SEM studies, these facies are identified as an early grain coating chlorite and a later pore filling chlorite. They have slightly different XRD patterns, which show the different origin. The change in diffraction pattern indicates that the relative amount of two types of chlorite varies in relation to reservoir properties.

## **Methods and Materials**

32 core samples of the Palaeocene Tyr Member sands in Rau-1A were studied by optical microscope, scanning electron microscope (SEM) to determine the rock composition and the diagenetic events such as mineral precipitation, dissolution, alteration and to evaluate the possible changes in petrology within the reservoir sand and across the oil water contact. Clay minerals were identified by XRD. XRF analyses were applied to supplement the existing database.

## **Results**

The investigated materials were core samples of Palaeocene sands referred to the Tyr Member from the well Rau-1A. Chlorite was formed as pervasive grain-coating cement, but much porosity was still present. In the oil zone and deeper, porous samples were later cemented by macroquartz, with larger amounts present in the water zone. Chlorite is found in varying amounts in Rau-1A samples. It can be recognized in SEM as a platy or bladed precipitate, which is mostly rich in Iron. Chlorite

is present in most samples, although only in traceable amounts in the samples, which are dominated by microquartz cement (Fig.1A).

There seem to be two chlorite phases: The first phase occurs as rosettes in a grain coating growth pattern. It is partially intergrown with microquartz or forms a dense mixture of small chlorite rosettes and scattered microquartz.

Pore-lining chlorite is partially post-compactional and grows into fractures in glauconite grains. Pore lining chlorite is formed prior to macroquartz and post-compactional calcite; whereas early calcite cemented samples (Fig.1A) did not evolve chlorite. The general impression is, however, that chlorite cement is more abundant and better developed in the lower parts of reservoir units, where as it may be scarce and poorly developed in upper parts, especially within the oil zone (Fig.1B). Below the oil-water contact, the growth of chlorite may have continued for a longer period, resulting in more dense coatings, which are very destructive for permeability. The second phase is characteristic of the very tightly cemented part above the oil zone in the upper reservoir unit. Above the oil zone the sandstone is cemented by a dense, grain coating microquartz cement, similar to what is seen in most studied samples (Fig.1C), but after cementation with microquartz, the remnant porosity was filled by irregular, bladed chlorite cement which seems to totally block the permeability. Above the oil-water contact, chlorite growth may have stopped at an earlier time, resulting in thin, sometimes discontinuous coating, but in many cases, there seem to be equal amounts of chlorite present. However, the chlorite may have evolved or collapsed to denser linings or lumps without the bladed surfaces (Fig.1D). The irregular bladed chlorite is known from other wells in the deeper part of the Siri Canyon, the Cecilie Field, and Augusta-1. It appears to be a late cement, probably also related to higher temperatures. It dominates in the uppermost part of the upper sand in Rau-1A, but this type is not important in the isolated sand above. The formation may have been controlled by influx rather than derivation from internal sources. This would have occurred prior to oil migration. Chlorite is also present in the water zone as dense cementation with chlorite (Fig.1E), where the preservation of porosity occurred and late cementation with pore filling chlorite blocks permeability. Pre-compactional calcite cement was precipitated in minor volume after growth of chlorite (Thin section.Fig.1F). It is generally patchy, leaving some open porosity left. In the uppermost part of sand unit 1 (above the oil zone) permeability has been lost due to dense, pore-filling chlorite cement, which can be distinguished from the pore-lining chlorite by its



morphology. The same morphological type is known from the Cecilie Field and from Augusta-1. It is assumed to be related to higher temperature, but still formed before oil migration.

On basis of SEM and petrographic studies, it is possible to suggest three different diagenetic phases in the studied well as below:

**Phase I:** Pre-compactional Calcite-Microquartz

**Phase II:** Chlorite, Post-compactional calcite-Macroquartz

**Phase III:** Chlorite

## **Discussion**

The Palaeocene Tyr member sandstone in Siri Canyon is an important hydrocarbon reservoir. However, in spite of its importance as a reservoir, published studies on Tyr member sandstone more specifically on the reservoir quality (including diagenesis), are very few. This study, which is based on core samples from the Rau-1A well in the Siri Canyon, reports the diagenetic characteristics of this reservoir. On basis of XRD data, it is possible to observe a slight shift of actual peak position in overlapped peaks of chlorite. Towards the top of the reservoir there is a shift to slightly larger d-spacings of the (002) and (004) chlorite peaks. This variation indicates two different facies of chlorite, and on basis of the SEM studies an early, grain coating chlorite and a late, pore filling chlorite can be identified. The distribution of these two types of chlorite in the well indicate that the slight shift in position of the (002) and (004) peaks relates to variation in the relative amounts of the two types of chlorite. The peaks are very closely spaced and overlapping. The shift to larger d-spacings correlates with increased proportions of the late, pore-filling chlorite(Fig.2). Grain-coating chlorites in clastic quartz-rich sandstones have long been recognized as an important porosity-preserving constituent in deep-burial diagenesis. Chlorite rosettes are partially intergrown with microquartz or forms a dense mixture of small chlorite rosettes and scattered microquartz.

Pore-lining chlorite is partially pre-compactional in the diagenetic history and grows into fractures in glauconite grains. Pore lining chlorite is formed prior to macroquartz and post-compactional calcite; whereas early calcite cemented samples did not evolve chlorite.

Late-stage authigenic clay minerals are pervasive in the very fine-grained, sandstones of the Tyr Member, comprising up to 38% of the bulk rock. Thus, reservoir rock properties are influenced by

these minerals. These studies have allowed to precise the diagenetic sequence for the formation and to approach the conditions for the formation of diagenetic chlorites for each case. In the topmost part of the reservoir unit, there is an increase in the amount of porefilling chlorite relative to the amount of porelining chlorite. The porefilling chlorite acts as an impermeable seal to hydrocarbon migration and prevents the topmost part of the reservoir to be oil filled. This part of the reservoir appeared to be more porous and permeable before the second phase of chlorite precipitation. This suggests that the formation of the intra-sandstone seal of diagenetic chlorite depends on variations in the flow pattern of the sandstone and relates to the distribution of early diagenetic microquartz (which preserve porosity and permeability), and early diagenetic chlorite which reduces the permeability. The high permeability zone in the topmost part of the reservoir sand was therefore more heavily cemented by the second phase chlorite and suffered a significant porosity and permeability loss. It must be expected that similar early cementation patterns may evolve intraformational seals as a response to late chlorite cementation. According to Stokkendal et al. (2009) dense cementation by microquartz is mainly expected close to upper or lower margin of sandstone units.

## **Conclusion**

The Tyr member sandstone is fine to medium-grained, moderate to well-sorted and glaucony-rich. The diagenetic processes recognized include compaction, cementation (calcite, clay minerals, quartz overgrowths, and a minor amount of pyrite), and dissolution of the calcite cements and of feldspar grains. The sandstone experienced the loss of some primary porosity at an early stage of diagenesis due to the precipitation of calcite cement. This early calcite cement, however, also partly helped to retain the porosity by resisting compaction of the sandstone at this stage. Post-compactional calcite cement was precipitated in minor volume after growth of chlorite. It is generally patchy, leaving some open porosity left in the water zone.

Based on the framework grain-cement relationships, precipitation of the early calcite cement was either accompanied or followed by the development of part of the pore-lining and pore-bridging chlorite cement in the oil zone.

Pore-filling chlorite resulted in a considerable loss of porosity and is a major cause for porosity-loss in the sandstone.

In the upper part of the reservoir, tight porefilling chlorite forms a reservoir seal. It formed as a response to the early cementation pattern with microquartz dominating close to the shale contact and porelining chlorite being more abundant in the remnant part of the reservoir. Porefilling chlorite is more abundant in the microquartz zone.

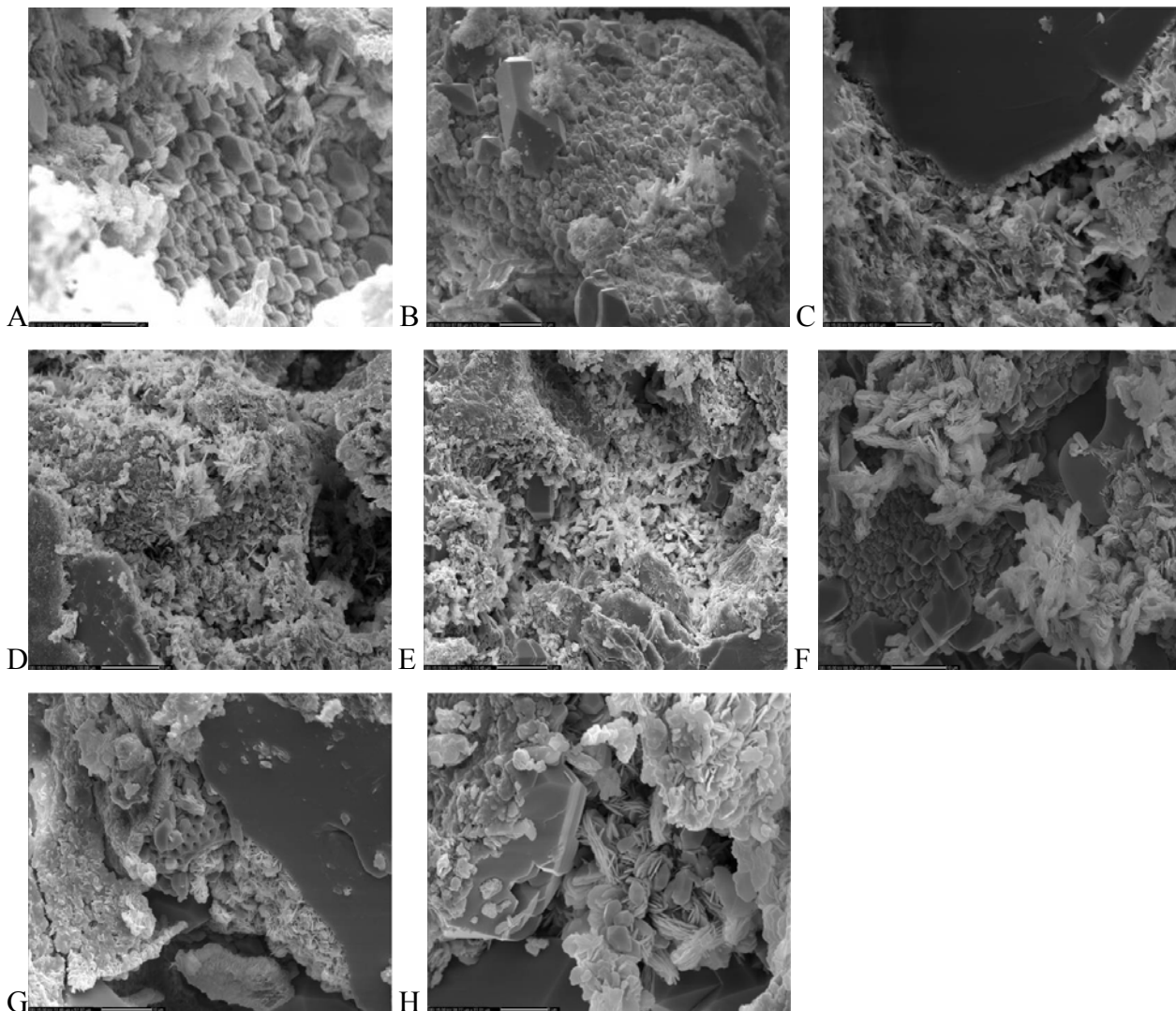


Figure 1. Scanning electron micrograph showing: (A) 256260m, quartz overgrowths consisting of small euhedral crystals locally developed in primary pores. (B) 256605m, Intergranular pore networks are often occluded by large quartz overgrowths. (C) 256620m, Quartz overgrowths enclosed chlorite plates, which also often interlock a narrow pore throats. Sometimes quartz overgrowths are inhibited by chlorite rims. (D) 256620, syntaxial quartz overgrowth, which eventually acts as pore occluding phase decreasing porosity and permeability. (E) 257230m, Pore lining chlorite fringes are developed in intergranular networks. (F) 257330m, grain coated chlorite rims on detrital grain. Chlorite also developed upon detrital mixed layer clay substrate. (G) 256930, Pore bridging chlorites act as barrier to fluid flow. (H) 256680m, chlorite coat on a detrital quartz grain, overgrown by euhedral quartz cement. Qz = quartz, Chl = chlorite.

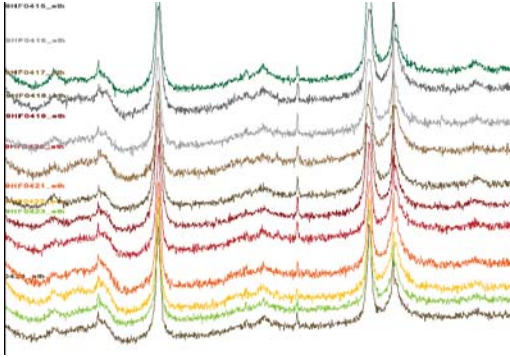


Figure 2. XRD diffractogram—On basis of XRD data it is possible to observe a slight shift of actual peak position in overlapped peaks of chlorite. Towards the top of the reservoir there is a shift to slightly larger d-spacings of the (002) and (004) chlorite peaks. This variation indicates two different facies of chlorite, and on basis of the SEM studies an early, grain coating chlorite and a late, pore filling chlorite can be identified. The distribution of these two types of chlorite in the well indicate that the slight shift in position of the (002) and (004) peaks relates to variation in the relative amounts of the two types of chlorite. The peaks are very closely spaced and overlapping. The shift to larger d-spacings correlates with increased proportions of the late, pore-filling chlorite.

### **Acknowledgments**

-Noreco-Danish North Sea Fund, State Participation in Oil and Gas Licences, RWE and Nordic Mineralogical Network (NMN).

## **Active silica sources in the Sele formation and quartz cementation in mudstone-Examples from the Siri Canyon, Danish North Sea**

A. M. Kazerouni<sup>1</sup>, H. Friis<sup>1</sup>, J. B. Svendsen<sup>2</sup>

1) *Department of Earth Sciences, Aarhus University*

2) *DONG Energy, Denmark*

### **Introduction**

The deep marine sandstones in the Siri Canyon (Fig.1) have been reported to import significant amounts of dissolved silica from adjacent Palaeocene shales during early diagenesis (Stokkendal et al. 2009; Weibel et al. 2010). We have studied the diagenesis of one of these shales, the Sele Formation shale to document the diagenetic steps which releases silica and to evaluate the possible timing of the silica export from the shale into neighbouring sandstones. The major silica mobilization occur at shallow depths, related to the transformation of biogenic opal and volcanic ash, and at intermediate depths, related to the dissolution of opal-CT and zeolite. At these processes, the shale may have been active silica exported. Reported sandstone cementation patterns indicate the earlier phase is related to major export of silica, whereas the shale itself was the major consumer during the intermediate phase. Late phase mobilization of silica (smectite to chlorite transformation) is at an initial stage and has not contributed significantly to the massive late-stage quartz cementation of the interbedded sandstones. The Sele Formation in the Siri Canyon has not been influence by illite formation, even at burial depth of approximately 3000 m. Potassium feldspar is not recorded, even at the shallowest depth, and we suggest that the lack dissolvable potassium sources has delayed the smectite transformation.

### **Discussion**

A major issue in this diagenesis study is the question of active silica sources for quartz cementation in sandstones and the timing of their active phases. Some of the suggested sources are internal, such as dissolution of feldspar or other silicate framework grain, or pressure solution at grain contacts in sandstones, pressure solution at stylolites in sandstones; others are external sources supplied by large-scale flow systems or supply from the adjacent shales by compactional flow or diffusion. There may be several silica sources in shale and they might be dynamic at different times during burial. Commonly cited silica sources are dissolution of quartz grains, opaline skeletal grains

(diatoms, radiolaria, sponge spicules), hydration of volcanic glass, conversion of smectite to illite during burial diagenesis, and decomposition of feldspars. Early cementation by opal and microquartz depends on the supply of dissolved silica from a readily dissolvable source. Silica release in shale does not necessarily source sandstone diagenesis but may re-precipitate as opal, quartz or other mineral phases inside the shale itself.

The process starts with biogenic silica dissolution and supersaturation of pore fluids with respect to opal-CT and quartz. Relative rates of opal-A and opal-CT nucleation govern the extent to which silica activity is buffered and hence the increase in surface area. From the point when further changes in specific surface area have negligible effect on opal-A solubility, opal-CT can form. With progressively less opal-A remaining, silica activity starts to decline and opal-CT nucleation becomes subordinate to growth. Opal-CT crystals with lower surface area form at the expense of smaller and less ordered ones.

Following the pathway during opal-A/ opal-CT transition. Precipitation of cryptocrystalline quartz began once the thermodynamic drive for the opal-CT became insignificant. Relative rates of opal-CT dissolution with respect to quartz nucleation and growth buffer the silica activity until it falls back towards the quartz solubility line with decreasing pore-water silica saturation. As the system evolves down this line, cryptocrystalline quartz is gradually replaced by epitaxial microcrystalline quartz.

The dominance of cryptocrystalline and microcrystalline quartz suggests that the dissolution rate of precursor phases (i.e. biogenic silica, opal-A and/or opal-CT) was fast enough to sustain silica saturation at the microquartz saturation level, resulting in numerous crystals instead of larger ones. Many studies have concluded that silica released as a result of clay mineral reactions in mudstones and shales is transported and precipitated as quartz cement in associated sandstones (e.g., Towe, 1962; Boles and Franks, 1979; Lynch et al., 1997; Land and Milliken, 2000; Van der Kamp, 2008).

## **Conclusion**

With-depth alteration the various components results in successive stages of silica-release. In shallow samples, the alteration of volcanic ash has already been completed. Released silica was

partly consumed for the precipitation of smectite and zeolite. Opal-CT is not systematically related to volcanic ash, and some silica may have been mobilized and migrated into interbedded sandstones. Also a major part of the biogenic silica has been transformed into opal-CT and partly to microcrystalline quartz. The microcrystalline quartz is an internal sink for dissolved silica, but the shale may have been an active silica exporter during this transition.

In the studied wells with deeper depth of burial, opal-CT is considered to be fully transformed to microcrystalline quartz. During this phase, silica has been partly mobile and depending on the rate of dissolution compared to the rate of precipitation, silica may have been lost to sandstone cementation. Zeolite was completely dissolved and its dissolution may also have mobilized silica and activated the shale as silica exporter.

At deep burial, iron-rich chlorite has replaced a minor part of smectite. The smectite to chlorite transformation released silica at the expense of iron. Therefore, a third phase of silica mobility was active. Microcrystalline quartz may have been an internal sink, but the shale would be also a potential silica supplier at this stage.

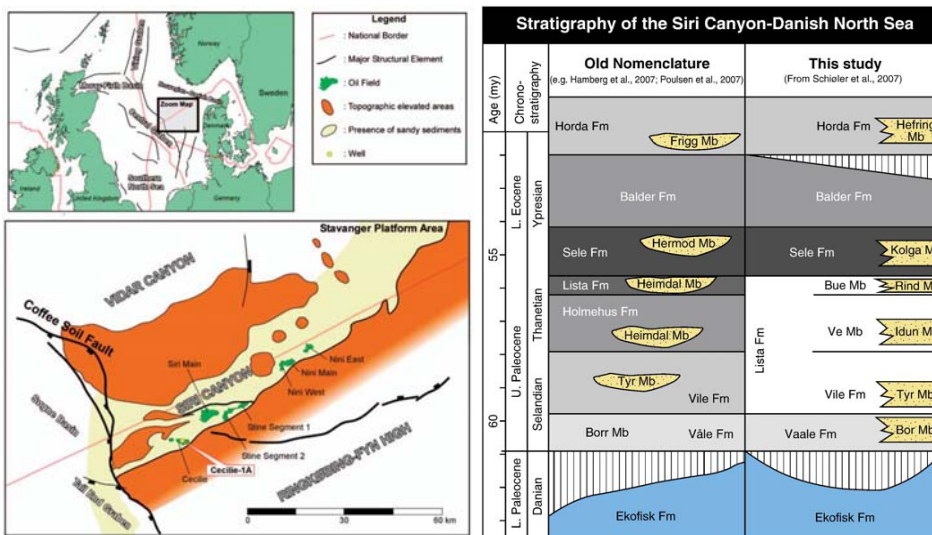


Figure 1. Geological setting & Location map of the Siri Canyon and wells investigated in the project. Stratigraphy of the Siri Canyon (Schiøler et al., 2007).

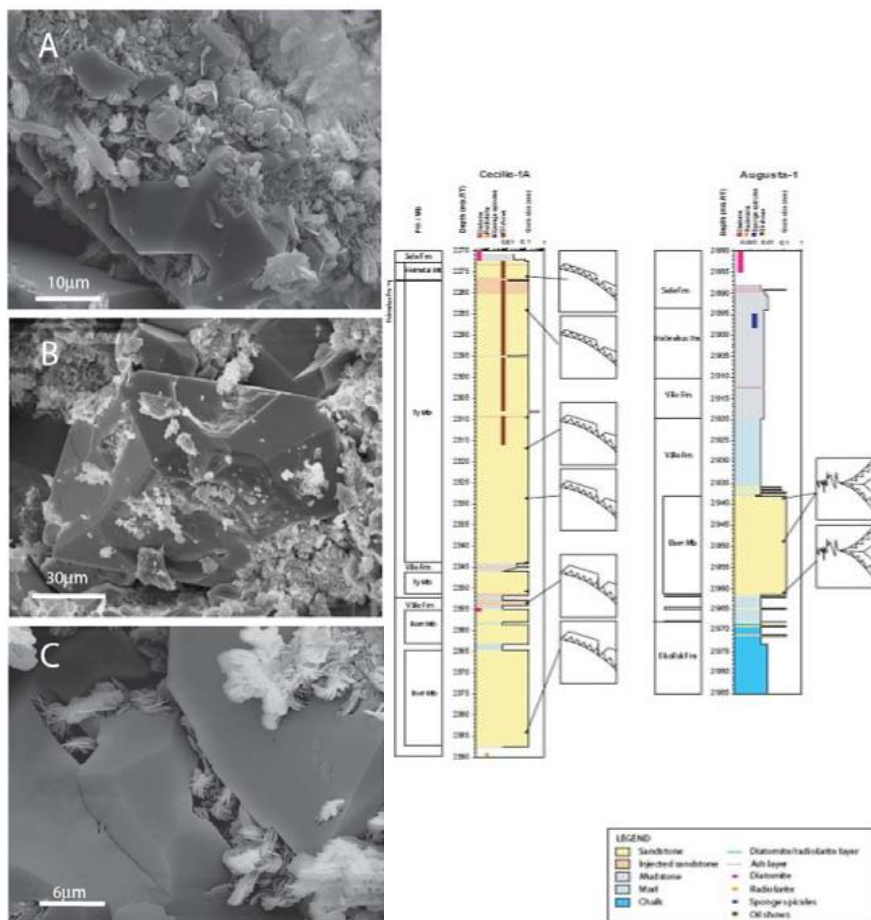


Figure 2. Macroquartz. A) Microquartz and macroquartz (together with authigenic chlorite) covering detrital quartz grain (Cecilie-1A, 2356.50 m, Bor Member); B) Detrital quartz grains completely enclosed in macroquartz (Augusta-1 2960.90 m, Bor Member); C) Macroquartz. (Cecilie-1 2300.50 m, Bor Member). Modified from Weibel et al. 2010.

## References

Boles, J. R. and Franks, S. G., 1979. Clay diagenesis in Wilcox sandstones of southwest Texas: Implications of smectite diagenesis on sandstone cementation. *Journal of Sedimentary Petrology*, 49, 55–70.

Land, L.S., Milliken, K.L. and McBride, E.F., 1987. Diagenetic evolution of Cenozoic Sandstones, Gulf-of-Mexico Sedimentary Basin. *Sedimentary Geology* 50 (1–3), 195–225.

Lynch, F.L., Mack, L.E. and Land, L.S., 1997. Burial diagenesis of illite/smectite in shales and the origins of authigenic quartz and secondary porosity in sandstones. *Geochimica et Cosmochimica Acta* 61 (10), 1995–2006.



Schiøler, P., Andsbjerg, J., Clausen, O.R., Dam, G., Dybkjær, K., Hamberg, L., Heilmann-Clausen, C., Johannesen, E.P., Prince, I. and Rasmussen, J.A., 2007. Lithostratigraphy of the palaeogene-lower neogene succession of the Danish North Sea. Geological Survey of Denmark and Greenland Bulletin 12, 5–77.

Stokkendal, J., Friis, H., Svendsen, J.B., Poulsen, M.L.K. and Hamberg, L., 2009. Predictive permeability variations in a Hermod sand reservoir, Stine Segments, Siri Field, Danish North Sea. Marine and Petroleum Geology 26, 397–415.

Towe, K.M., 1962. Clay mineral diagenesis as a possible source of silica cement in sedimentary rocks. Journal of Sedimentary Petrology 32 (1), 26–28.

Van der Kamp, P.C., 2008. Smectite–illite–muscovite transformations, quartz dissolution, and silica release in shales. Clays and Clay Minerals 56 (1), 66–81.

Weibel, R., Friis, H., Kazerouni, A.M., Svendsen, J.B., Stokkendal, J. and Poulsen, M.L.K., (in press) Development of early diagenetic silica and quartz morphologies - Examples from the Siri Canyon, Danish North Sea, Sedimentary Geology. doi:10.1016/j.sedgeo.2010.04.008.

## **Partial replacement of alite by Klein's compound: An approach to reduce cement related CO<sub>2</sub> emissions? A laboratory study**

Maria Rosenberger Rasch<sup>1a,1b</sup>, Hans Dieter Zimmermann<sup>2</sup>, Duncan Herfort<sup>3</sup>, Lise Frank Kirkegaard<sup>2</sup>

1a) *Dept. of Earth Sciences, Aarhus Universitet, DK-8000 Århus C, Denmark*

1b) *Nørrealle 24, DK-8000 Århus C (email: rasch.maria@gmail.com)*

2) *Dept. of Earth Sciences, Aarhus Universitet, DK-8000 Århus C, Denmark (email: geolhans@geo.au.dk)*

3) *Aalborg Portland, Product Technology, Rørdalsvej 44, DK-9220 Aalborg, Denmark*

### **Introduction**

Cement production is heavy on the global anthropogenic carbon dioxide budget. No other industry comes anywhere near emitting as much CO<sub>2</sub>. The production of Portland cement is estimated to cause 6 - 7% of the total global anthropogenic emission of CO<sub>2</sub> and is expected to double within the next 30 years (Damtoft et al., 2008). Therefore, the cement industry is facing a challenge and is looking for ways to reduce its discharge of the greenhouse gas CO<sub>2</sub>.

On average, 0.96 tons CO<sub>2</sub> gas are released per ton cement. The major portion, 0.58 t, is due to the calcination of limestone. Limestone is CaCO<sub>3</sub>. It is the most important raw material for cement and provides the CaO, the dominant component in cement clinker. The principal clinker phase is alite (C<sub>3</sub>S). It is the phase with the highest Ca content.

### **Possible partial replacement of alite by Klein's compound**

One possible approach for a more CO<sub>2</sub>-efficient cement production is the partial replacement of alite by a less Ca-rich clinker phase. Klein's compound (C<sub>4</sub>A<sub>3</sub> $\bar{S}$ ) could be a suitable substitute (Gartner, 2004). However, it does not normally coexist with alite. Therefore, alite must be stabilised in the presence of Klein's compound. Following up on Liu et al. (2003), Odler & Schmidt (1980) and Knöfel (1978), we have tried to do this by using zinc as mineralizing agent. Likewise, we have experimented with the addition of minor concentrations of strontium and fluor.

### **Starting materials**

The oxide weight percentages of our basic starting material were CaO 58, SiO<sub>2</sub> 17, Al<sub>2</sub>O<sub>3</sub> 14, SO<sub>3</sub> 7, K<sub>2</sub>O 1. From this, we prepared samples of seven different compositions by adding Zn (as ZnO), Sr (as SrO), Sr+F (as SrO + CaF<sub>2</sub>) and F (as CaF<sub>2</sub>) in concentrations between 0.25wt% and 2 wt%. The samples were burnt at 1100C, 1200C, 1300C and 1400C. The run products were analysed by XRF, XRD and on the electron microprobe. Quantitative phase analysis was obtained by Rietveld analysis.

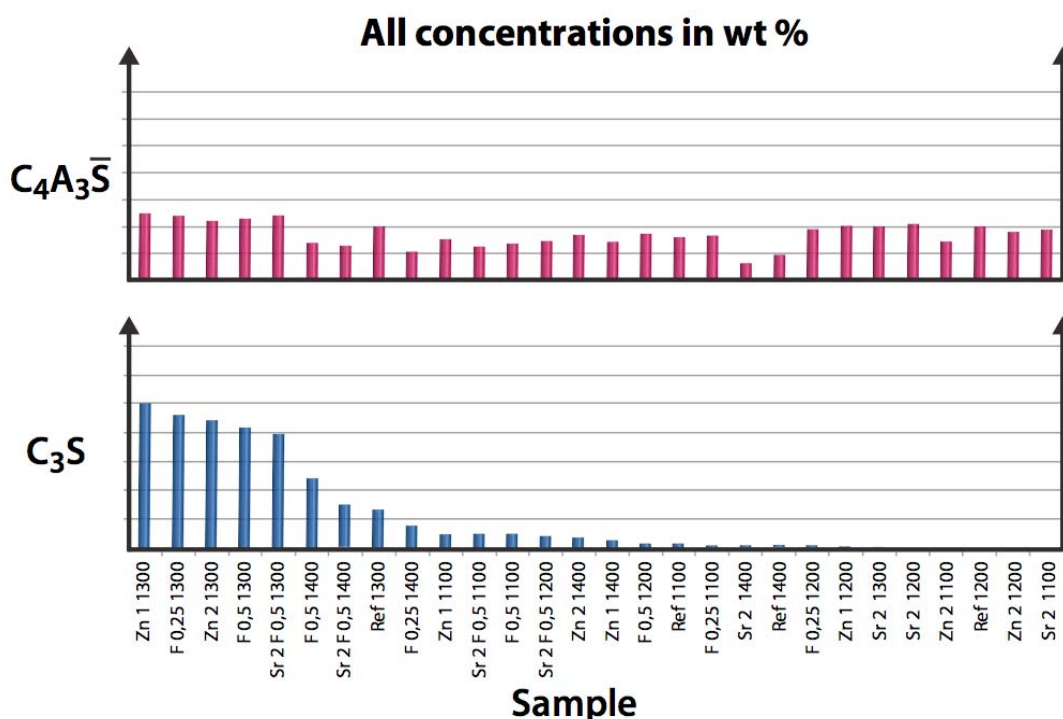


Figure 2. Concentrations of coexisting alite (C<sub>3</sub>S) and Klein's compound (C<sub>4</sub>A<sub>3</sub>S̄). Horizontal lines represent concentration levels in weight percents in steps of 10. – Legend for added mineralisers: Zn1 og Zn2: 1 og 2 wt% ZnO; Sr2: 2 wt% SrO; F0.25 og F0.5: 0.25 og 0.5 wt% CaF<sub>2</sub>; Sr2F0.5: 2 wt% SrO + 0.5 wt% CaF<sub>2</sub>; Ref: reference sample, no mineralisers added.

## Results

The main results are summarized in Fig. 1. Our experiments suggest compatibility of of alite with Klein's compound at 1300 C (Fig. 2) for compositions with Zn, F and Sr + F. The weight percentages of the main phases in these run products are alite 42 – 50, Klein's compound 22 – 25

and belite 25 – 33. Adding strontium alone does not favour the phase association alite – Klein’s compound, rather seems to destabilise it.

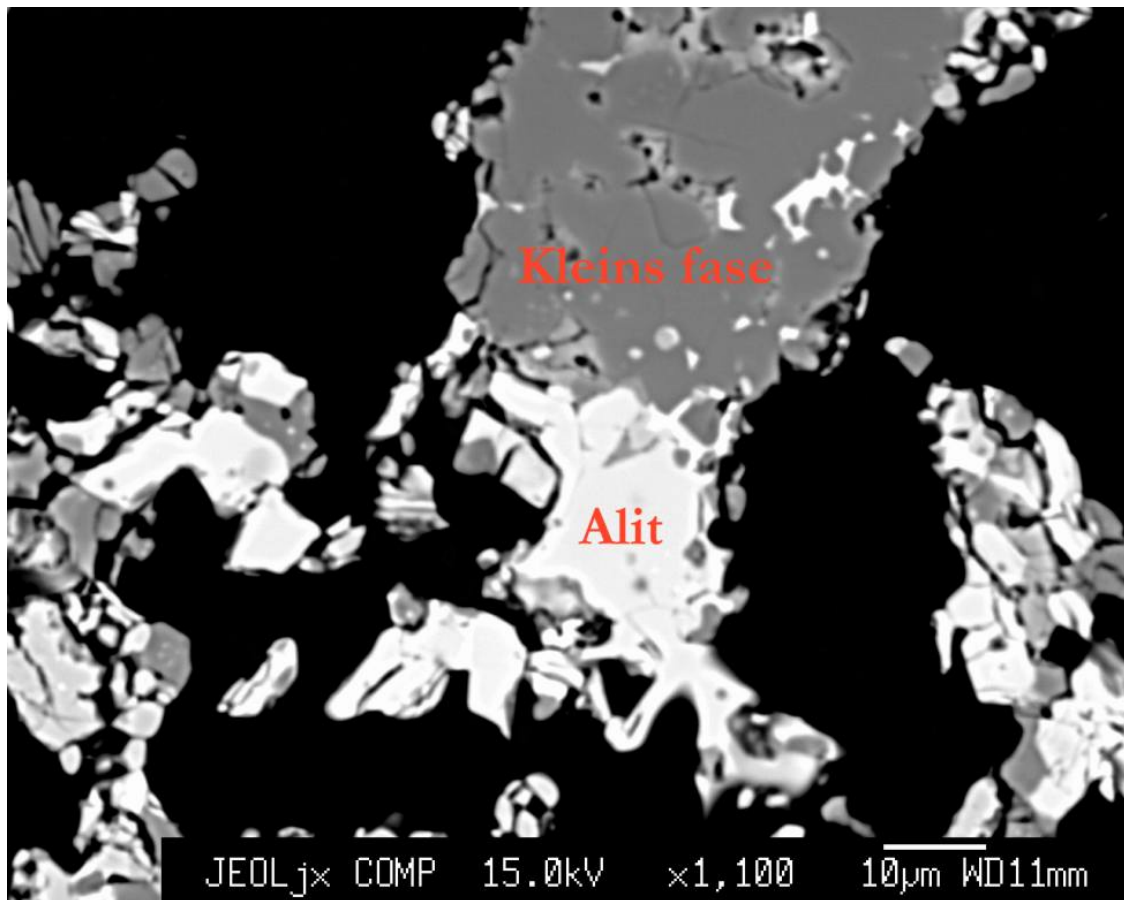


Figure 2. Back-scattered electron image of clinker burnt at 1300 C. Coexistence of alite (bright whitish phase, in the lower middle) and Klein’s compound (medium grey, upper middle).

## References

Damtoft, J.S., Lukasik, J., Herfort, D., Sorrentino, D. and Gartner, E.M., 2008. Sustainable development and climate change initiatives. *Cement and Concrete Research*, 38, 115-127

Gartner, E., 2004. Industrially interesting approaches to “low-CO<sub>2</sub>” cements. *Cement and Concrete Research*, 34, 1489-1498.

Knöfel, D., 1978. Modifying some properties of Portland cement clinker and Portland cemen by means of ZnO and ZnS. *Zement-Kalk-Gips*, 3.

Liu, X.-C., Li, Y.-J., 2003. Influence of ZnO and/or CaF<sub>2</sub> on Mineral Formation of C<sub>3</sub>S and C<sub>4</sub>A<sub>3</sub> $\bar{S}$ .  
Journal of Building Materials 6, 1.

Odler, I. and Schmidt, O., 1980. Structure and properties of Portland cement clinker doped with zinc oxide. J. Am. Ceram. Soc. 63(1-2), 13-16.

## **PGM and PGE alloy nuggets- and Au-nuggets from alluvial deposits in Finnish Lapland**

Ragnar Törnroos<sup>1</sup> and Kari Kojonen<sup>2</sup>

1) *Department of Geosciences and Geography, Division of Geology, University of Helsinki, POBox 64, FI-00014 University of Helsinki, Finland (e-mail: ragnar.tornroos@helsinki.fi*

2) *Geological Survey of Finland: POBox 96, FI-02151 Espoo, Finland, (e-mail: kari.kojonen@gtk.fi)*

Placer gold has been recovered from the Ivalojoiki river area since 1870 and from 1945 on from tributaries in the Lemmenjoki river area (localities shown on the map in Fig.1). The studied placer gold and platinum-group element (PGE) mineral nuggets are separated from heavy-mineral concentrates supplied to us by several miners working these placer deposits for gold. The placer deposits consists of glaciofluvial river gravels, sands and terraces and basal till and weathered bedrock surface of the Paleoproterozoic ca. 2 Ga granulite complex of Finnish Lapland.

The granulite complex of northern Finland forms an arc that extends north-south from the Norwegian border and intersect the Russian border in an east-west direction (Fig. 1). This arc is bordered in the southwest by Archaean greenstones, quartzo felspathic schists and gneisses. The NE-SW trending river valleys define the main fault and shear zones that cut the general strike of the strongly strained metasedimentary and magmatic rocks. Smaller creeks define shear zones subparallel to shallowly NE dipping foliation.

The amount of gold panned in 1870-1910 was 464 kg, and the total amount recovered from placers in Lapland since 1870 is ca. 1000 kg. In 2009 panning operations were active in the Ivalojoiki, Tolosjoki, Härkäselkä, Tankavaara, Laanila and Lemmenjoki areas.

The form of the Au nuggets is angular, rounded or flat. The Au content in the core of the nuggets range from about 72 to 100 wt.%, Ag 0-27 wt.% and Cu 0 - 0.2%. Sporadically Fe up to 0.6 wt% and traces of S, As, Sb, Te, Bi, Ni, and Pt are met with. The rims of the nuggets are often depleted in Ag. A few composite Au-Ag alloy (electrum) nuggets occur in the Lemmenjoki area. Some nuggets contain platinum, palladium and mercury. As inclusions in the gold nuggets occur native Bi, bismuthotellurides, Fe-Ni-Co arsenides and sulpharsenides, Fe-Cu-Mo-Pb sulphides, Cr-Fe-Ti oxides and hydroxides (e.g. arsenopyrite, gersdorffite, pyrite, pyrrhotite, chalcopyrite, galena, molybdenite, ilmenite, Fe-oxides, limonite, goethite), mafic silicates (e.g. amphibole, pyroxene,

chlorite). Other inclusions observed in the gold nuggets are quartz, siderite, and kaolinite. The gold nuggets are commonly covered with limonite or Mn-oxide crust and tiny gold grains occur within limonite and Fe-oxides as inclusions. Not uncommon are also gold-Fe-oxide nuggets containing microscopic gold inclusions. Native gold has been previously observed in the cross-cutting quartz-, quartz-carbonate, hematite- and quartz-feldspar porphyry veins.

Alluvial nuggets of PGE alloys from the rivers Miessijoki, Sotajoki and Ivaloiki have been investigated by microprobe and scanning electron microscope. Several nuggets are large in size, up to several mm, but also very small ones are present. Mostly the material is well rounded due to transport, but in some nuggets the original euhedral form can be observed clearly indicating crystal structure (Fig. 2). Pt-Cu, Pt-Cu-Au and Os-Ir-Ru alloys occur as well as Pt-Fe and Pt-Fe-Cu alloys (Fig 3). The alloys occur both as inclusions in the Pt-Fe alloy but also as separate nuggets or crystals (Fig 2C). The inclusions in the nuggets show a marked variation in number and size. Several PGE sulphides, including the very common laurite occur. The Os-Ir-Ru-Pt alloys occur either as idiomorphic platy crystals 0.5 - 1.0 mm in size or as zoned lath-formed prismatic or platy inclusions in isoferroplatinum or Pt-Fe alloys. Cuprian platinum occur as mixed grains 0.2-2 mm wide, as nuggets and/or as exsolution lamellae together with Pd-Au, Pt-Cu-Au and complex Pt-Fe alloys. All Pt-Cu alloys are anisotropic. Pd-Au alloys occur as idiomorphic crystals 0.1-0.5 mm wide together with other Pd and Pt minerals and alloys. Cu is always present in small amounts and may build up together with Pd, Au and Pt a series of alloys of very different compositions (e.g. Fig. 3).

A total of 43 PGE mineral phases were discovered in the heavy mineral sands occurring together with Au and Au-Ag alloy grains, garnet, monazite, zircon, pyrite, Cr-Fe-spinel, magnetite, ilmenite, rutile, hematite, columbite-tantalite, tapiolite, uraninite-thorianite, galena, Pb-Sn alloy, wolframite, amphiboles and pyroxenes. The PGE minerals exist as individual grains or as inclusions in larger PGM grains (Törnroos and Vuorelainen, 1987, Törnroos et al. 1996, Kojonen et al. 2005). The PGM:s consist chiefly of sperrylite  $PtAs_2$ , Pt-oxide, native Pt, and isoferroplatinum  $Pt_3Fe$ . So far has 23 unknown or undefined PGM and Au-phases been detected by means of microprobe analyses in the nuggets (Table 2).

Several sulphides occur as inclusions while some silicates and oxides are especially common at grain boundaries, as well as within nuggets, including ilmenite, magnetite,  $TiO_2$ , "limonite", titanite,

zircon, albite, kaolinite, almandine-grossular, feldspar, tremolite, quartz and calcite. The most common of these are kaolinite, limonite and titanium oxides, suggesting a lateritic stage in placer development and probable *in situ* formation of some of the PGM nuggets. The other silicate inclusions are indicative of a mafic source.

The great variety of PGE minerals, the native Au, the Au-Ag alloys and their inclusions suggests a complex and multi-stage crystallisation - mineralisation in the source rocks from magmatic to hydrothermal conditions, followed by secondary weathering, oxidation and nugget growth in the regolith profile (Kojonen et al. 2005, Törnroos et al. 2006). The PGE mineral paragenesis points to a close source. Gold and PGM concentrated during weathering, erosion, glaciofluvial and fluvial processes from the layered amphibole-pyroxene rocks, volcanogenic greenstones and hydrothermal quartz-carbonate veins, especially occurring in the Miessijoki and Sotajoki (Ivalojoiki) areas. The oxides, quartz and siderite occurring together with gold may indicate that the placer gold originates from local hydrothermal veins composed mainly of quartz and siderite and quartz and hematite. However, the microscopic intergrowth textures of limonite with tiny native gold inclusions suggest secondary nugget growth in the regolith profile during weathering and short transport from the regolith source (Lawrance 2001).

## References

Kojonen, K., Tarkian, M., Knauf, V.V. and Törnroos, R. 2005. New results of the placer PGE-minerals from Ivalojoiki and Lemmenjoki rivers, Finnish Lapland. 10th Int. Platinum Symp. Oulu, Finland, Abstract Vol., 145-149.

Kojonen, K., Tarkian, M., Roberts, A.C., Törnroos, R. and Heidrich, S. 2007. Miessiite, Pd<sub>11</sub>Te<sub>2</sub>Se<sub>2</sub>, a new mineral species from Miessijoki, Finnish Lapland, Finland. Canadian Mineralogist, 45, 1221-1227.

Lawrance, L.M. 2001. Multi-element dispersion within salt-lake environments: case study of the buried Hannan South gold deposit, Western Australia. Geochem. Exp. . Env. Anal. 1. 323-339.

Törnroos, R. and Vuorelainen, Y. 1987. Platinum-group metals and their alloys in nuggets from alluvial deposits in Finnish Lapland. Lithos 20, 491-500.



Törnroos, R., Johanson., B. and Kojonen, K. 1996. Alluvial nuggets of platinum-group minerals and alloys from Finnish Lapland. IGCP Project 336, Symposium, Rovaniemi Finland, Program and Abstracts p.86-86.

Törnroos, R., Kojonen, K, Tarkian, M.and Kivioja, K. 2006. New observations of the Au and PGE nuggets in the Ivalojoiki and Lemmenjoiki areas, Finnish Lapland. Nordic Geological Wintermeeting, Oulu, Program and Abstracts p. 71.

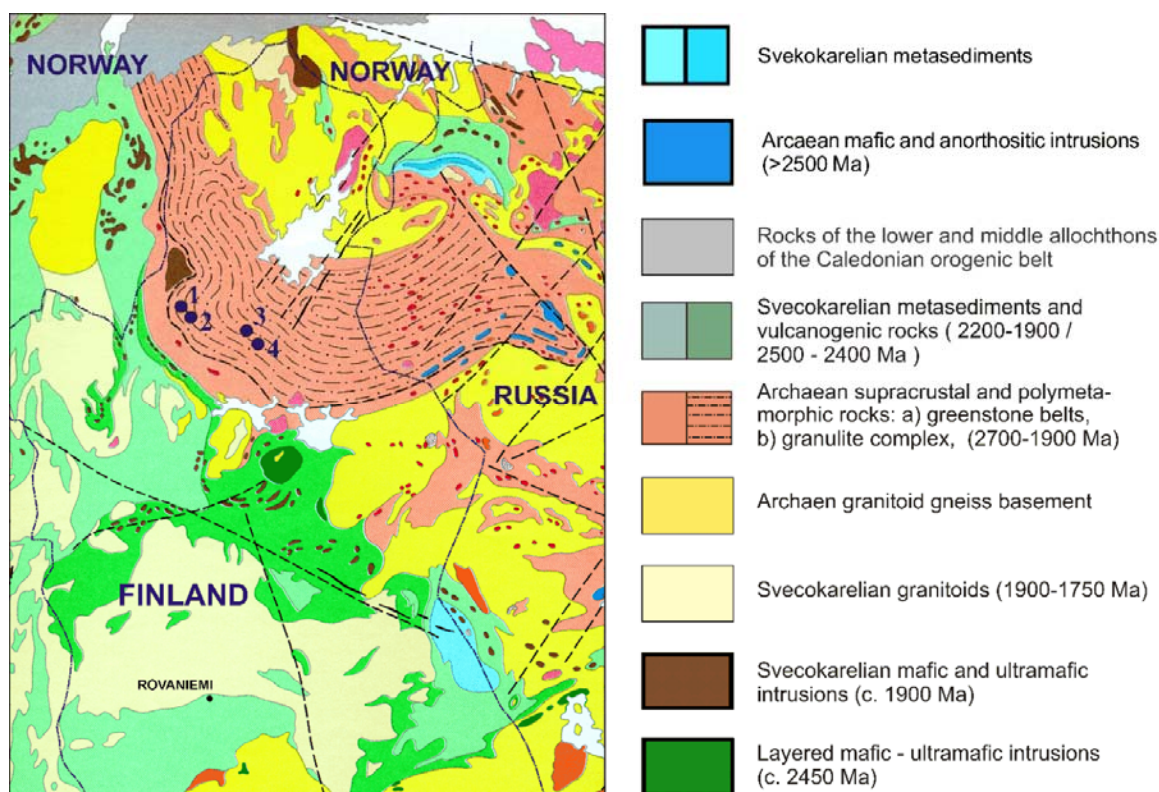


Figure 1. Map of northern Finnish Lapland showing the alluvial deposits at 1 Miessijoki, 2 Puskuoja, 3 Sotajoki, 4 Härkäselkä area

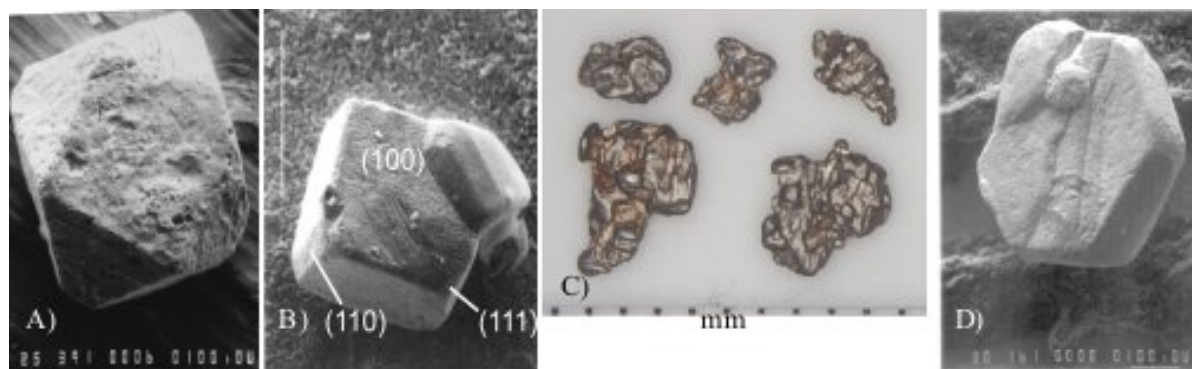
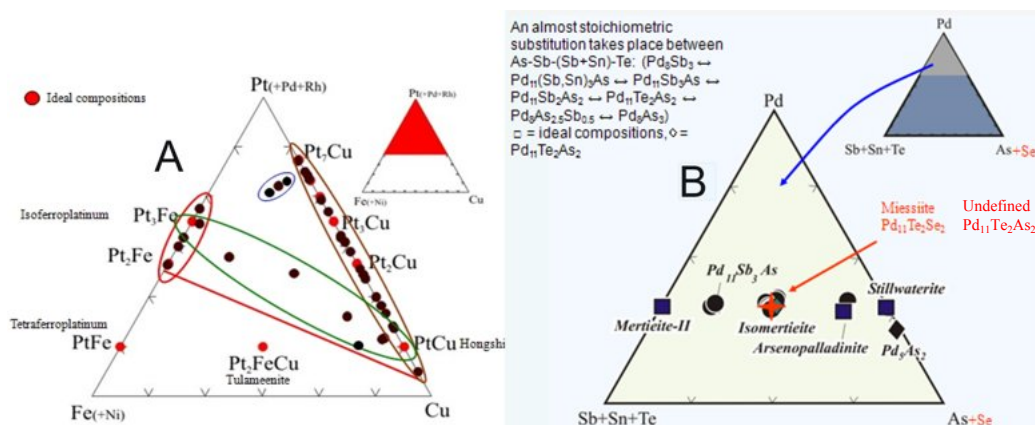


Figure 2. Crystals and nuggets of PGM:s. A) Sperrylite, B) and C) Isoferroplatinum, D) Mertieite crystal with tiny gold, Miessijoki Length of bars 100  $\mu$ m



**TABLE 2. Undefined PGE phases found in alluvial nuggets from Lapland**

Empirical formulae based on microprobe analyses	Ideal
1. $[Pt_{0.99}Rh_{0.01}Cu_{0.01}(Pd,Os,Ag)_{0.01}]_{1.02}(Te_{0.97}Sb_{0.01}Sn_{<0.01})_{0.98}$	PtTe
2. $(Pt_{1.83}Ir_{0.02}Rh_{0.02}Os_{0.01}Pd_{0.01}Au_{0.11}Ag_{0.02})_{2.02}Cu_{0.98}$	Pt <sub>2</sub> Cu
3. $(Pt_{2.77}Rh_{0.02}Os_{0.02}Pd_{0.01}Au_{0.06}Ag_{0.01})_{2.89}Cu_{1.08}Fe_{0.01}$	Pt <sub>3</sub> Cu
4. $(Pt_{4.89}Pd_{0.05}Rh_{0.04}Os_{0.02})_{5.00}(Cu_{1.94}Fe_{0.02})_{1.96}(As,Te,Sb,Sn,S)_{0.04}$	Pt <sub>5</sub> Cu <sub>2</sub>
5. $(Pt_{6.71}Pd_{0.06}Rh_{0.05}Os_{0.03}Ir_{0.04}Ru_{0.01}Ag_{0.06})_{6.97}(Cu_{0.98}Fe_{0.03})_{1.01}(Bi_{0.01}As_{0.01}Te_{0.01})$	Pt <sub>7</sub> Cu
6. $(Pt_{5.79}Pd_{0.12}Rh_{0.06}Os_{0.02}Ag_{0.02})_{6.01}Fe_{1.05}Cu_{0.85}(Ni,Sn,Sb,Te,As)_{0.09}$	Pt <sub>6</sub> FeCu
7. $(Pt_{3.93}Rh_{0.03}Os_{0.02}Fe_{0.01}Ni_{0.01}Cu_{<0.01})_{4.00}(Pd_{0.97}Ag_{0.03}Sn_{<0.01}Te_{<0.01})_{1.00}$	Pt <sub>4</sub> Pd
8. $Pt_{8.70}Pd_{1.16}(Os,Rh,Cu,Fe)_{0.13}$	Pt <sub>9</sub> Pd
9. $(Pd_{4.86}Pt_{0.03}Ir_{0.01}Ag_{0.01}Au_{<0.01})_{4.91}[As_{2.08}(Sn,Te,S)_{0.01}]_{2.09}$	Pd <sub>5</sub> As <sub>2</sub>
10. $[Pd_{10.94}(Pt,Os,Ir,Rh,Au,Ag,Fe,Ni,Cu)_{0.07}]_{11.01}[Te_{1.63}Sb_{0.30}(Sn,S)_{0.09}]_{2.02}As_{1.98}$	Pd <sub>11</sub> Te <sub>2</sub> As <sub>2</sub>
11. $\left. \begin{array}{l} [Pd_{10.8}(Pt,Os,Ir,Rh,Au,Ag,Fe,Cu)_{0.13}]_{10.95}Sb_{2.85}As_{0.90}Te_{0.30} \\ [Pd_{10.92}(Pt,Os,Ir,Au,Ag)_{0.10}]_{11.02}Sb_{3.02}Te_{0.06}As_{0.90} \end{array} \right\}$	Pd <sub>11</sub> Sb <sub>3</sub> As
12. $(Pd_{10.96}Os_{0.01}Ir_{0.01}Ag_{0.03}Ni_{0.01}Cu_{0.05})_{11.07}(Sb_{2.41}Sn_{0.56})_{2.97}(As_{0.85}Bi_{0.07}Te_{0.05})_{0.97}$	Pd <sub>11</sub> (Sb,Sn) <sub>3</sub> As
13. $Pd_{10.97}(Sb_{1.67}As_{1.40})_{3.07}Sn_{0.92}$	Pd <sub>11</sub> (Sb,As) <sub>3</sub> Sn
14. $Pd_{7.88}Pt_{0.03}Au_{0.02}Cu_{0.01}Ir_{0.01})_{7.95}As_{2.61}Sb_{0.44}$	Pd <sub>8</sub> (As,Sb) <sub>3</sub>
15. $(Au_{0.97}Pb_{0.03})_{1.00}(Sn_{1.98}Se_{0.01}Bi_{<0.01})_{1.99}$	AuSn <sub>2</sub>
16. $Au_{1.97}(Pd_{0.75}Cu_{0.19}Ag_{0.08}Sb,Fe,S)_{1.03}$	Au <sub>2</sub> (Pd,Cu,Ag)
17. $(Au_{3.98}Ag_{0.03})_{4.01}[Cu_{0.95}(Fe,Bi,S)_{0.05}]_{1.00}$	Au <sub>4</sub> Cu
18. $Au_{4.09}(Pd_{0.60}Cu_{0.25}Ag_{0.05}Pt_{0.01})_{0.91}$	Au <sub>4</sub> (Pd,Cu,Ag)
19. $(Au_{3.80}Ag_{0.09})_{3.89}(Pd_{0.75}Cu_{0.35})_{1.10}$	(Au,Ag) <sub>4</sub> (Pd,Cu)
20. $(Au_{5.88}Ag_{0.14})_{6.02}Pd_{0.98}Cu_{0.94}$	(Au,Ag) <sub>6</sub> PdCu
21. $Au_{5.98}(Pd_{0.90}Pt_{0.04}Ir_{0.05}Cu_{0.02})_{1.01}Ag_{1.00}$	Au <sub>6</sub> PdAg
22. $Au_{6.02}[Pd_{0.41}Cu_{0.39}(Pt,Ir,Ru,Ni,Fe,Ag)_{0.13}]_{0.97}$	Au <sub>6</sub> (Pd,Cu)
23. $Au_{6.07}(Pd_{0.77}Ag_{0.09}Cu_{0.05}Sb_{0.01}As,S)_{0.93}$	Au <sub>6</sub> (Pd,Ag,Cu)

Figure 3. A) Analyses in the system Pt(+Pd+Rh) – Fe(+Ni) – Cu showing an extensive solid solutions range of Pt and Cu from PtCu to Pt<sub>7</sub>Cu (brown), and for PtFe in the range Pt<sub>2</sub>Fe to Pt<sub>3</sub>Fe (red) and Pt–Fe–Cu (green) between PtCu to Pt<sub>3</sub>Fe. In the range (blue) Pt<sub>7</sub>Cu – Pt<sub>3</sub>Fe there are so far three analyses. So far no compositions below the red line have been found. B) Analyses in the system Pd–Sb+Sn+Te – As+Se with the new mineral Miessite and the new phase Pd<sub>11</sub>Te<sub>2</sub>As<sub>2</sub>.

## Heavy minerals from gold sluicings in Lapland Gold Rush areas, and their bearing on the origin of gold bearing tills

Pekka Tuisku<sup>1</sup>

1) *Department of Geosciences, university of Oulu, 90014 University of Oulu, Finland (Email: pekka.tuisku@oulu.fi)*

### Lapland gold rushes



Figure 1. A) Kultalan Kruunun Stationi at Ivalojoiki, B) Gold sluicing at Ivalojoiki near Kruunun Stationi.

The gold rush to Lapland started in 1868 when gold nuggets were found in Nulkkamukka at Ivalojoiki. The Grown Gold Station or “Kultalan Kruunun Stationi” (Fig 1A) was founded on the Ivalojoiki bank for state officers keeping order and collecting taxes of panned gold in the gold rush area. According to tax accounting, annual gold production in the first years was 56 kg which has a current value of 1.86 m€. In the beginning of 20th century there was an increased prospecting of possible bedrock gold, the “second gold rush” (Fig 1B). The bedrock prospecting, however, was unsuccessful and the founded prospecting companies were bankrupted. The third gold rush to Lapland started 1945 when gold nuggets were found in un-accessible wilderness of Lemmenjoki (Partanen 2005).

### Heavy minerals

Heavy minerals as garnet, PGE-minerals and corundum among others are found commonly as by-product of gold panning and sluicing in the gold rush areas of Ivalojoiki and Lemmenjoki (Törnroos and Vuorelainen 1987, Kojonen et al. 2006, 2007, Lahtinen 2008, Törnroos and Kojonen 2010, Tuisku and Lahtinen 2010). These are used in jewelry and by collectors. Corundum, PGM and PGE have never been found in the granulite-facies regional metamorphic bedrock of the gold rush area while other heavy minerals as garnet, ilmenite, rutile, monazite and zircon are common in granulites (Tuisku and Huhma 2006, Tuisku et al. 2006). The problem of the source-rock for heavy minerals



touch also the enigma of bedrock provenance of gold as the minerals occur in the same soil, mostly glacial till (Fig 2) (Forsström and Tuisku 1990, 1993).



Figure 2. Images of gold-bearing soils in sluicing sites of Lapland gold rush areas. A) Clayey unsorted till at Suolaoja, Ivalojoiki area. Note the red and yellowish brown shades of the soil due to the abundant lateritic material and absence of sorting. B) Poorly washed clayey till at Ellioja, upper course of Palsioja, Ivalojoiki area. Oriented boulders indicate SW transport of the drift. C) Clayey unsorted till at the river bank, lower course of Palsioja, Ivalojoiki area.

### Sluicing samples and their enrichment

In this study fine grained leftover black sand samples were taken from the riffles of sluices after removal of larger gold nuggets. Although these sands may contain considerable amounts of fine gold and minerals of platinum group elements, the sands are usually considered as “waste” because it has been difficult to extract gold from this material in field conditions. The samples were enriched by GOLD MINER Spiral Gold Panning Machine and the two fractions obtained; 1) almost pure gold or gold with variety of heavy minerals and 2) black sand with only small amounts of gold were both weighed. Small amounts of fractions were scattered on carbon tape and about 500 – 1000 grains of each sample were identified by scanning electron microscope equipped with EDS.

### Heavy mineral patterns of sluicing samples

Heavy mineral patterns of sluicing samples may be used for drawing conclusions on the nature of the parent rock or in the best case for identification of the parent. Heavy mineral compositions of three samples are reported here; enriched gold-rich fraction from Jäkälä-Äytsi, Lemmenjoki area, enrichment residue of the same sample and enriched fraction from Rapeli at upper course of Miessijoki, Lemmenjoki area (Table 1). It may be seen, that minerals with specific weight over 3.5 seem to be enriched in the black sand during gold sluicing (i.e. pyrope, almandine etc.). It is also seen, comparing the Jäkälä samples that minerals with  $D < 4.7$  tend to be left in residue and those

with  $D > 5.4$  tend to be enriched in the heavy fraction while monazite, which typically has density between 4.9 – 5.4 is split between the residue and the concentrate during spiral panning.

The other important observation is that Jäkälä and Rapeli samples have considerably different heavy mineral pattern although the distance between the two sites is only 3.5 km.

Jäkälä1	Au-rich fraction	
	grains	%
Au	379	77.0
Fe	8	1.6
Monazite-Ce	49	10.0
Fe-Al-silicate	3	0.6
Ferberite	1	0.2
Sperrylite	17	3.5
Ilmenite	3	0.6
Taenite	1	0.2
Magnetite	9	1.8
Hematite	13	2.6
Tongxinite	1	0.2
Zircon	3	0.6
Cuprite	1	0.2
Isoferroplatinum	1	0.2
AuAg	3	0.6
	492	100.0

Jäkälä1	Left over after Au removal	
	grains	%
Au	1	0.2
Monazite-Ce	150	29.9
Fe-Al-silicate	1	0.2
Ilmenite	191	38.1
Magnetite	7	1.4
Hematite	25	5.0
Tongxinite	2	0.4
Zircon	67	13.4
Rutile	10	2.0
Ilmenohematite	2	0.4
Almandine	17	3.4
Pyrope	28	5.6
	501	100.0

Rapeli	grains	%
Au	125	16.4
Fe	2	0.3
Monazite-Ce	148	19.4
Ferberite	4	0.5
Sperrylite	352	46.3
Ilmenite	10	1.3
Magnetite	20	2.6
Hematite	33	4.3
Zircon	2	0.3
Isoferroplatinum	1	0.1
AuAg	6	0.8
Ilmenohematite	1	0.1
Almandine	2	0.3
Tantalite-Fe	25	3.3
Tantalite-Mn	7	0.9
Bismite	4	0.5
Fergusonite-Y	1	0.1
Lithic	1	0.1
Columbite-Fe	1	0.1
Thorianite	3	0.4
Calcite	1	0.1
Braggite	2	0.3
FeNi	1	0.1
Pt	1	0.1
Al-silicate	1	0.1
CuZnNi	1	0.1
Cassiterite	1	0.1
Cobaltarthurite	1	0.1
Grossular	1	0.1
AuCu	1	0.1
Quartz	1	0.1
Biotite	1	0.1
	761	100.0

Table 1. Heavy mineral content of some black sand samples after spiral panning. Left: Spiral enrichment of black sand from creek Jäkälä-Äytsi, Lemmenjoki area. Center: Panning residue of the same sample. Right: Spiral enrichment of black sand from Rapeli-Kangas claim at upper course of Miessijoki, Lemmenjoki area.

## Parent rocks

Heavy minerals in the studied samples may be divided to two parts, those that are typical for the bedrock of the area and the atypical ones. Iron and titanium oxides belong to the first group as rutile, ilmenite and ilmenohematite are common in metapelitic granulites and magnetite in enderbites of

the area. Also the amphibolites of the SW marginal zone of the granulite belt contain abundant Fe- and Ti-oxides. Same applies to garnets and, monazite and zircon are common in metapelitic migmatites (Tuisku and Huhma 2006, Tuisku et al. 2006). Most of the mineral species are, however rare or never found in the bedrock of the area. These may be divided to three parts, firstly those that are more common in basic lithologies, and secondly those that are commonly encountered in siliceous rocks, as complex pegmatites etc. The former group includes minerals of platinum group elements and the latter tantalite, columbite, ferberite, cassiterite, fergusonite, and also monazite and zircon. Third group consist of apparently heavenly objects as iron, FeNi and taenite.

## **Conclusion**

The list of heavy mineral and abundance of them do not indicate any specific mineral association occurring in gold ores and the mother rock of gold must still be considered somewhat enigmatic. However, the mineral associations may be used to trace glacial drift directions and they also give indication of possible economic deposit types of the area and give thus useful guide for exploration. The possible ore types in the source area might be those of Nb, Ta, Sn and rare earth elements and, on the other hand PGEs, in addition of gold ores.

It may be concluded that a great part of the heavy mineral grains were transported by glacial drift outside their present finding site and the area of granulite-facies bedrock. Transport of several kilometres is necessary for some of them but some minerals might have a local bedrock provenance from the granulite belt.

## **Acknowledgements**

This work could not have been possible without the valuable work of several gold miners in Lapland. Special thanks for Janne Kannisto and Olavi Lind for samples and field guidance.

## **References**

Forsström, L. and Tuisku, P. 1990. Missä on Lapin kullin emäkallio?. Summary: Where is the mother rock for the gold of Lapland to be found? *Geologi* 42, 147-150.

Forsström, L. and Tuisku, P. 1993. Lapin irtokullan paikallisuudesta ja kulkeutumisesta. Summary: On the local nature of Lapland placer gold and its transport. *Geologi* 45, 71-76.

Kojonen, K., Tarkian, M., Knauf, V. V., Törnroos, R. and Heidrich, S. 2006. Placer platinum-group minerals from Ivalojoiki and Lemmenjoiki rivers, Finnish Lapland. In: Program & abstracts of the 19th General Meeting of the International Mineralogical Association, Kobe, Japan, July 23-28, 2007, p. 196.

Kojonen, K., Tarkian, M., Roberts, A.C., Törnroos, R. and Heidrich, S. 2007. Miessiite, Pd<sub>11</sub>Te<sub>2</sub>Se<sub>2</sub>, a new mineral species from Miessijoki, Finnish Lapland, Finland. *The Canadian Mineralogist* 45 (5), 1221-1227.

Lahtinen, K. 2008. Lapin korundin alkuperä. *Res Terrae Ser. B*, No 19, 81 p.

Partanen, S., 2005. Ivalojoiki : kulkijan kultamaa. Hipputeos Ltd. 128 p.

Törnroos, R. and Kojonen, K. 2010. PGM and PGE alloy nuggets- and Au-nuggets from alluvial deposits in Finnish Lapland. This volume.

Törnroos, R. and Vuorelainen, Y. 1987. Platinum-group metals and their alloys in nuggets from alluvial deposits in Finnish Lapland. *Lithos* 20 (6), 491-500.

Tuisku, P. and Huhma, H. 2006. Evolution of Migmatitic Granulite Complexes: Implications from Lapland Granulite Belt, Part II: Isotopic dating. *Bulletin of the Geological Society of Finland*, 78, 143–175.

Tuisku, P. and Lahtinen, K. 2010 Origin of corundum in Lapland. This volume.

Tuisku, P., Mikkola, P. and Huhma, H. 2006. Evolution of Migmatitic Granulite Complexes: Implications from Lapland Granulite Belt, Part I: Metamorphic geology. *Bulletin of the Geological Society of Finland*, 78, 71–105.

## Origin of corundum in Lapland

Pekka Tuisku<sup>1</sup> and Kimmo Lahtinen<sup>1,2</sup>

1) *Department of Geosciences, university of Oulu, 90014 University of Oulu, Finland (Email: pekka.tuisku@oulu.fi)*

2) *Talvivaara Exploration Ltd, Talvivaarantie 66, 88120 Tuhkakylä, Finland (Email: Kimmo.Lahtinen@talvivaara.com)*

### Lapland gold rushes

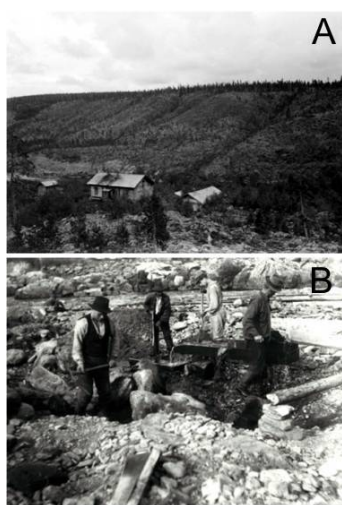


Figure 1. A) Kultalan Kruunun Stationi at Ivalojoiki, B) Bedrock prospecting at Sotajoki

A The gold rush to Lapland started in 1868 when gold nuggets were found in Nulkkamukka at Ivalojoiki. The grown gold station or “Kultalan Kruunun Stationi” (Fig 1A) was founded on the Ivalojoiki bank for state officers keeping order and collecting taxes of panned gold in the gold rush area. According to tax accounting, annual gold production in the first years was 56 kg which has a current value of 1.86 m€. In the beginning of 20th century there was an increased prospecting of possible bedrock gold, the “second gold rush” (Fig 1B). The bedrock prospecting, however, was unsuccessful and the founded prospecting companies were bankrupted. The third gold rush to Lapland started 1945 when gold nuggets were found in un-accessible wilderness of Lemmenjoki.

### Corundum

Heavy minerals as garnet, PGE-minerals and corundum among others are found commonly as by-product of gold panning and sluicing in the gold rush areas of Ivalojoiki and Lemmenjoki. Corundum is used in jewelry and by collectors although most of the produced grains are not gem quality. However some red ruby (Fig 2A) and blue sapphire is found. Other useful semi-precious stones include Lapin tähti Fig 2B) and schiller-corundum (Fig 2C). Corundum has never been found in outcrops of the gold rush area although the granulite-facies regional metamorphism of the bedrock is quite providential for the generation of it. The problem of the source-rock for corundum touch also the enigma of bedrock provenance of gold as the two minerals occur in the same soil,



mostly glacial till (Fig 3).



Figure 2. Corundum grains from Lapland gold rush areas. A) Euhedral ruby from Jäkälä-Äytsi, Lemmenjoki area. Sample G, diameter 5 mm. B) Lapin tähti (star of Lapland) corundum from Palsioja a tributary of Ivalojoiki, Ivalojoiki area. Sample M, diameter 25 mm. D) Corundum having zonal pronzeous luster as a result from arrangement of Schiller inclusions (hematite) which most probably were formed by exsolution in the  $Al_2O_3$ - $Fe_2O_3$ -system. Polished sample Miessi I1, diameter 15 mm.



Figure 3. Images of soils in sluicing sites of Lapland gold rush areas. A) Clayey unsorted till at Suolaoja, Ivalojoiki area. Note the red and yellowish brown shades of the soil due to the abundant lateritic material and absence of sorting. B) Poorly washed clayey till at Ellioja, upper course of Palsioja, Ivalojoiki area. Oriented boulders indicate SW transport of the drift. C) Clayey unsorted till at the river bank, lower course of Palsioja, Ivalojoiki area.

## Inclusions

Inclusions and parent-rock fragments of corundum may be used for drawing conclusions on the nature of the parent rock or in the best case for identification of the parent. It may also be possible to conclude whether various corundum types have different parent rocks or whether provenance of corundum is different in different areas or deposits. Similarly inclusions may provide evidence on the crystallization path of corundum and thus evolution of the parent. Inclusions with abundant radioisotopes may be used to draw conclusions on the age of the parent and even on the evolution of the parent. It is amazing that these methods have never been used before during the 150 years of exploration for the mother rock for Lapin Kulta (Gold of Lapland). The inclusions consist mostly of margarite and chlorite and to lesser extend of muscovite and biotite in the majority of the samples. Inclusions in schiller-corundum mostly consist of oxides as hematite, ilmenite and rutile and phosphates monazite and apatite and also some zircon. Rare inclusion assemblages include K-feldspar + chrysoberyl, garnet + aluminium silicate etc. (Fig 4) (Lahtinen, 2008).

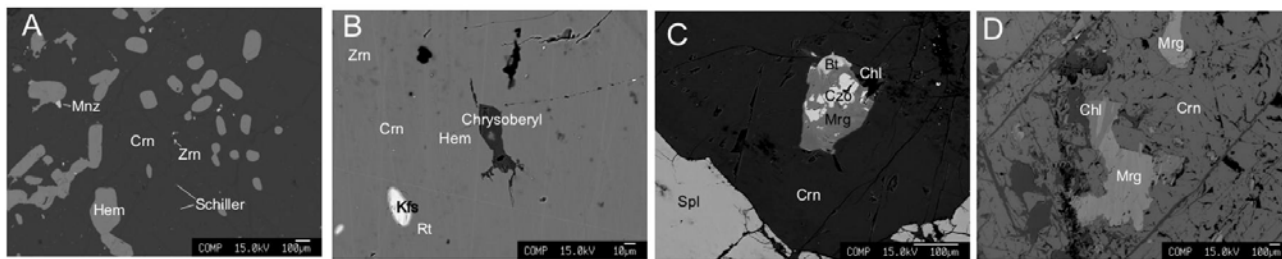


Figure 4. BE-images of inclusion in corundum grains from Lapland gold rush areas. A) Hematite grains and schiller lamellae, monazite and zircon in pronze zoned corundum from Selperinoja, Ivalojoiki area (Sample Zellberg). B) K-feldspar and chrysoberyl in pale red translucent corundum from Hangasoja, Ivalojoiki area (sample Hangasoja). C) Clinozoisite, biotite, chlorite and margarite in red jewel ruby from Miessijoki, Lemmenjoki area (sample Miessi1). D) Margarite and chlorite in red ruby from Uusihaara, Ivalojoiki area (sample UusihaaraB).

### Isotopic dating

Zircons and monazites were dated from different corundum types and different areas. Monazites were invariably about 1900 Ma old which is exactly the age of regional metamorphism in the area (Tuisku & Huhma, 2006). It may be concluded that all monazite bearing corundum grains are derived from regional metamorphic rocks of the area or syn-metamorphic igneous rocks. Concordant zircon U-Pb ages fall in three groups 1900 Ma, 1940 Ma and Archaean. Abundant discordant zircon grains are found in schiller-type corundum, but they seem, however, to fall in line between Archaean (~2600 Ma) and Palaeoproterozoic (1900 Ma) age on the concordia suggesting a (partial) lead loss of Archaean zircons at 1900 Ma or before.

### Parent rocks

The oxidized nature of schiller-type corundum samples and the dominance of the most weathering resistant minerals suggest that schiller-corundum grains were derived from metamorphosed lateritic deposits that were metamorphosed during Palaeoproterozoic era before tertiary parent-rock weathering and exposition to quaternary glaciations. These are thus samples with evidence of two extensive lateritic weathering periods, the Palaeoproterozoic and Tertiary ones. The monazite ages (1900 Ma) and zircon ages (concordant 2600 and 1900 Ma and discordant lead loss line between 2600 and 1900 Ma) suggest that the weathered rocks represent Archaean basement, weathering was Palaeoproterozoic and weathering crust was metamorphosed at 1900 Ma, leading to lead loss of recycled and partially weathered zircon grains.

The possible source rock of the corundum having 1940 Ma old zircon could be an igneous rock because no regional metamorphic event of this particular age is known in the whole Shield.

Speculative sources could be alkaline rocks of oceanic crust as some ophiolites of the area or the only known rocks of that age known so far. Interesting sample was found from Miessijoki, a tributary of Postijoki and Vaskojoki. A Large fragment of side-rock was found in this high quality ruby. We formulated a model for the side rock chemistry from the side minerals (spinel, pargasite, and chlorite) and calculated a possible PT-evolution for this hypothetical rock from inclusion and replacement relations of corundum. Evidently the evolution consists of a clockwise PT-path very similar to that calculated for SW marginal zone of Lapland Granulite Belt by Tuisku & al. (2006). It is Probable that this ruby was generated in silica poor mafic metavolcanite of the marginal zone during regional metamorphism at 1900 Ma.

## **Conclusion**

It may be concluded that most of the corundum grains were transported by glacial drift outside their present finding site and area of granulite-facies bedrock. Transport of over 20 km is necessary for some of them but some; especially those found from Miessijoki in Lemmenjoki area might be relatively local as the area is situated nearby the SW marginal zone. From mineralogy and isotopic dating it is evident that corundum grains have several source rocks but that most of the crystals were generated due to the 1900 Ma regional metamorphism of the area.

## **Acknowledgements**

This work was supported financially by K.H. Renlund Foundation. Special thanks for Janne Kannisto, Risto Häkkinen and Olavi Lind for samples and field assistance.

## **References**

- Lahtinen, K. 2008. Lapin korundin alkuperä. Res Terrae Ser. B, No 19, 81 p.
- Tuisku, P. and Huhma, H. 2006. Evolution of Migmatitic Granulite Complexes: Implications from Lapland Granulite Belt, Part II: Isotopic dating. Bulletin of the Geological Society of Finland, 78, 143–175.
- Tuisku, P., Mikkola, P. and Huhma, H. 2006. Evolution of Migmatitic Granulite Complexes: Implications from Lapland Granulite Belt, Part I: Metamorphic geology. Bulletin of the Geological Society of Finland, 78, 71–105.

## **Geochemistry and P–T conditions of magnetite quartzites from Jõhvi Zone, NE Estonia**

Margus Voolma<sup>1</sup>, Alvar Soesoo<sup>1</sup> and Sigrid Hade<sup>1</sup>

1) *Institute of Geology at Tallinn University of Technology, Ehitajate tee 5, 19086 Tallinn, Estonia; E-mail: margus.voolma@gi.ee; alvar.soesoo@gi.ee; sigrid.hade@gmail.com*

The Estonian Precambrian basement can be considered as a southern continuation of the Fennoscandian Shield of the East European Craton. This basement comprises two major units: amphibolite facies rocks of northern Estonia, which are similar to the rocks of southern Finland; and mostly granulite facies rocks of southern Estonia, which form a part of the Belarus-Baltic Granulite Belt. On the basis of geophysical and petrological studies, six structural-geological zones can be distinguished within these major units: the Tallinn, Alutaguse and Jõhvi Zones in northern Estonia, and the West Estonian, Tapa and South Estonian Zones in southern Estonia (Fig. 1). Since the crystalline rocks are covered by 100-700 m thick sedimentary cover, geological information on the crystalline rocks in Estonia comes mostly from studies of drill core material and geophysical studies.

The Jõhvi zone is a narrow 20–30 km wide and 100 km long complex in NE Estonia, characterized by strong E–W trending magnetic anomalies and positive gravity anomalies. The complex consists of pyroxene gneisses and inter-layered quartz-feldspathic gneisses, biotite-plagioclase gneisses, amphibole gneisses, garnet-cordierite gneisses, and magnetite quartzites. Migmatization is widespread, resulting in the formation of veins and small bodies of rocks that have granitic, charnockitic and enderbitic composition. Generally these rocks have formed under the conditions of granulite facies metamorphism (Soesoo et al. 2004). The Jõhvi magnetite quartzites occur as subvertical beds in garnet-cordierite or pyroxene gneisses. Seven drillcores out of 18 in the area of Jõhvi Magnetic Anomaly (JMA) contain magnetite quartzites. Drill core study shows that the complex of gneisses and magnetite quartzites is about 100 m thick. Magnetite quartzites occur as lenses (Suuroja 1969).

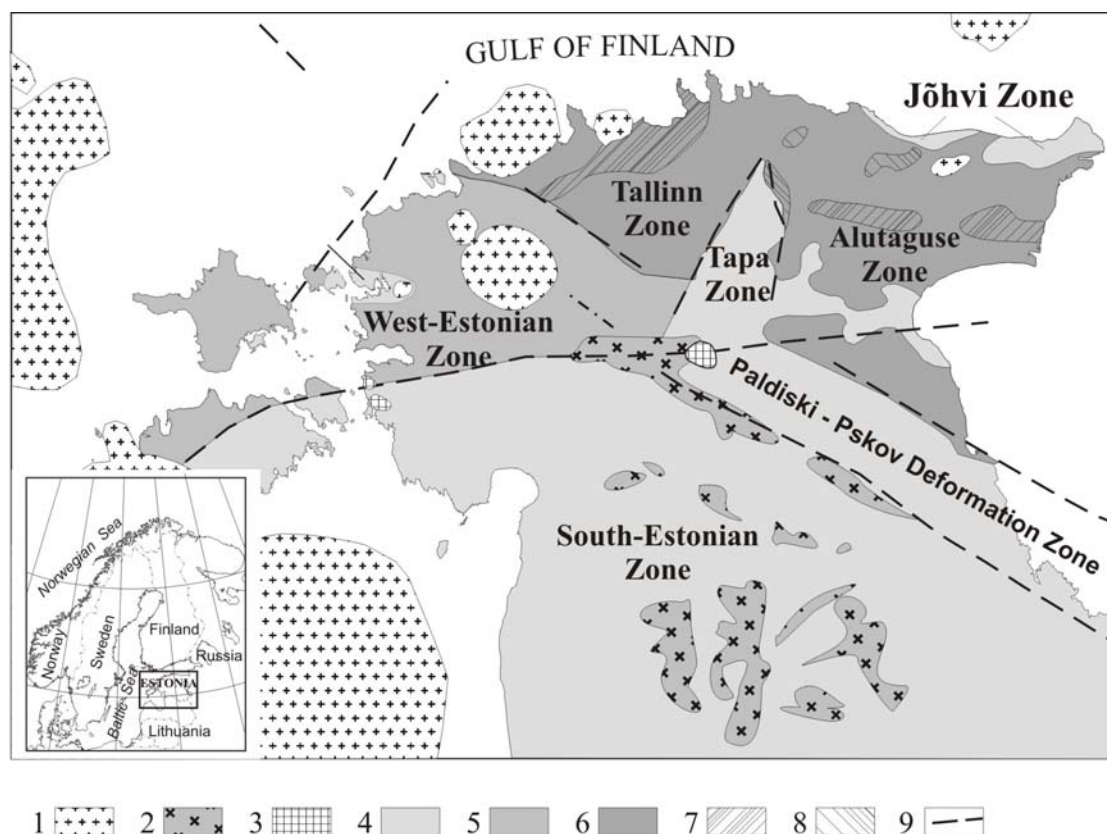


Figure 1. Geological outline of Estonian Precambrian basement with structural zones. 1 – Rapakivi intrusions; 2 – Microcline granitoids; 3 – Postorogenic intrusions; 4 – Areas with dominant granulitic facies metamorphism; 5 - Areas with dominant retrograde metamorphism facies; 6 - Areas with dominant amphibolite facies metamorphism; 7 – Low grade amphibolite facies; 8 – High grade amphibolite facies; 9 – Shear and thrust zones.

Nine magnetite quartzite samples from drill cores F1 (N59° 22,766'; E27° 30,220') and F12 (N59° 22,849'; E27° 34,281') were analysed for whole rock composition (XRF) and mineral chemistry (SEM). Metamorphic pressures and temperatures were calculated by using garnet–biotite geothermometer and garnet–biotite–plagioclase–quartz (GBPQ) geobarometer. Magnetite quartzites are very fine grained manganiferous rocks with thin foliated beds/layers where quartz is alternating with dark minerals. Samples from drillcore F12 are more massive. Mineral assemblages are  $qtz\text{--}mt\text{--}grt\pm bt\pm px\pm amf\pm fsp$ . Accessory minerals are zircon, monazite, apatite, titanite, ilmenite, pyrite, sphalerite, calcopyrite, allanite, and uraninite. Garnet and feldspar grains occur as porphyroblasts

which often have pressure shadows of magnetite or quartz. Magnetite and quartz are disseminated between other minerals. Garnets are 0.1–0.3 mm, anhedral, sometimes elongated and contain inclusions of zircon, quartz and monazite. Composition of garnet in drillcore F12 is  $Alm_{60-74}Pyr_{20-26}Gross_{4-7}Spess_{3-10}$ . The variations in composition from core to rim are small. The  $X_{Mg}$  (Mg/Fe+Mn+Mg+Ca) is 0.20-0.25. There are two types of garnets in drillcore F1. One is similar to

drillcore F12 Alm<sub>62</sub>Pyr<sub>11</sub>Gross<sub>5</sub>Spess<sub>23</sub>, but slightly richer in manganese and less magnesium-rich. Other garnets are Alm<sub>27-34</sub>Pyr<sub>2</sub>Gross<sub>20-28</sub>Spess<sub>40-46</sub>. Garnets in which spessartine component dominates are usually found in some skarn deposits, they frequently occur in manganese-rich assemblages with rhodonite, pyroxmangite, tephroite of metasomatic origin associated either with adjacent igneous intrusions or with a more widespread regional metamorphism (Deer 1992).

Biotite is commonly iron-rich. The  $X_{Mg}$  ( $Mg/Fe+Mg+Ti+Al^{VI}$ ) is 0.46–0.55. In sample F12910 the  $X_{Mg}$  is the lowest - 0.35 as in garnets from the same sample. Plagioclase is andesine with a composition of An<sub>35-46</sub>Ab<sub>52-62</sub>Or<sub>2-3</sub>. Feldspar is mostly microcline and orthoclase. Plagioclase from sample F122547 has high iron content (in contact with garnet). The small amount of Fe<sup>2+</sup> sometimes recorded must be considered either as an impurity or as replacing Ca. The pyroxene belongs to the series diopside–hedenbergite–johannsenite. Intermediate members between diopside and hedenbergite occur in regionally metamorphosed calcium-rich sediments and basic igneous rocks in higher grades of the amphibolite facies (Deer 1992). Hedenbergite occurs as a product of contact-metamorphosed iron-rich sediments. Johannsenite, commonly associated with rhodonite and bustamite, occurs as a skarn mineral in metasomatized limestones associated with the formation of copper, zinc and lead ores (Deer 1992). Ilmenite from samples F122788 and F123369 contains about 30-35 wt% MnO, 40-45 wt% TiO<sub>2</sub> and 10-20 wt% FeO and in F13090 about 5-6 wt% MnO. In coexisting ilmenite and magnetite in igneous and metamorphic rocks, MnO is always preferentially found in the ilmenite. Manganesian ilmenite is usually found in granitic rocks and also in some carbonatites. In solid solution between ilmenite and pyrophanite (MnTiO<sub>3</sub>) the pyrophanite may become important in ilmenites in differentiated acid rocks and in carbonatites (Deer 1992). In sample F13090 apatite grains are euhedral with diameter 0.3 mm and contain inclusions of monazite. Sample F13090 contains 2 wt% P<sub>2</sub>O<sub>5</sub>, while other samples have P<sub>2</sub>O<sub>5</sub> concentrations up to 0.7 wt%, averaging 0.13 wt%. Another characteristic feature of magnetite quartzites is their high manganese content which ranges from 0.3 wt% to 15.8 wt%, with an average of 3 wt%. Sulfur content is the highest in samples from drillcore F1, reaching about 1 wt%.

There are nearly 30 versions of the garnet–biotite thermometers at present, among which the Holdaway (2000) version yields the smallest absolute error ( $\pm 25^{\circ}\text{C}$ ) in reproducing the experimental temperatures of Ferry & Spear (1978) and Perchuk & Lavrent'eva (1983), in the wide temperature range of 550–950 °C (Wu et al., 2004). Metamorphic temperatures were calculated by the Holdaway 2000 grt–bt geothermometer and Nakamura 2009 grt–cpx geothermometer. The activity

models are those used by the authors. Aluminosilicate minerals are not always present. In this case the widely used garnet–aluminosilicate–plagioclase–quartz (GASP) barometer cannot be applied. Wu et al. calibrated the garnet–biotite–plagioclase–quartz (GBPQ) barometer, so that it may be applied to metapelites, especially when aluminosilicate is absent. Metamorphic pressures for the studied rocks were calculated by the grt–bt–pl–qtz (Wu et al., 2004) geobarometer. With the above geothermobarometers the metamorphic temperatures and pressures obtained were  $650\pm 50$  °C and 4.3–5.6 kbars (sample F122547 2.9 kbar).

The Jöhvi magnetite quartzites and associated rocks can be compared with those of the Bergslagen area. By far the most common type of metallic mineral deposits in Bergslagen consists of iron oxide with variable amounts of Mn in associated skarn and crystalline carbonate rocks. More than 2000 deposits are known, most of which are small and, since the middle of the 19th century, without any economic significance. The economically important iron oxide deposits in Bergslagen may be subdivided into the following categories: iron oxide deposits in Mn-poor and Mn-rich skarn and carbonate rocks, quartz-rich iron oxide deposits including banded iron formations (BIF), and apatite-bearing iron oxide deposits. The term “skarn” is used non-genetically and refers to calc-silicate or Mg-silicate mineral assemblages. In addition, iron oxide deposits associated with high contents of sulphides of base metals are present. Above-mentioned iron oxide types may be considered as end members, and characteristics corresponding to more than one type are locally found in different places of, or along strike, in the same deposit. For example, some iron oxide skarn deposits appear to grade into quartz-rich iron deposits (Allen et al. 2008). It can be speculated here that the Jöhvi Zone may be a continuation of Bergslagen. Based on geochemical and mineralogical evidence magnetite quartzites from the Jöhvi Zone represent different types of iron deposits which are similar to iron deposits occurring in Bergslagen.

## References

- Allen, R., Ripa, M. and Jansson, N. 2008. Palaeoproterozoic Volcanic- and Limestonehosted Zn-Pb-Ag-(Cu-Au) Massive Sulphide Deposits and Fe oxide deposits in Bergslagen, Sweden. 33 IGC excursion No 12, August 14 – 20.
- Deer, W. A., Howie, R. A. and Zussman, J. 1992. An Introduction to the Rock Forming Minerals. Pearson Ed. Ltd., 2<sup>nd</sup> ed., 696 p.

Nakamura, D., 2009. A new formulation of garnet–clinopyroxene geothermometer based on accumulation and statistical analysis of a large experimental data set. *J. metamorphic Geol.*, 27, p. 495–508.

Soesoo, A., Puura, V., Kirs, J., Petersell, V., Niin, M. and All, T. 2004. Outlines of the Precambrian basement of Estonia. *Proc. Estonian Acad. Sci. Geol.*, 53/3, 149 -164 p.

Suuroja, K., 1969. „Jõhvi magnetiitse maagistumise iseloomust” PhD thesis, Tartu, 88 p.

Wu, C., Zhang, J. and Ren, L., 2004. Empirical Garnet – Biotite – Plagioclase – Quartz (GBPQ) Geobarometry in Medium- to High – Grade Metapelites. *Journal of Petrology*, vol. 45, nr. 9, p 1907 – 1921.



## **Optical Mineralogy – An Anachronism?**

Hans Dieter Zimmermann

*Dept. of Earth Sciences, Aarhus Universitet, DK-8000 Århus C (email: geolhans@geo.au.dk)*

### **Polarised light microscopy and knowledge of rocks**

To a large extent, our knowledge of rocks is based on studies with polarised light microscopy (PLM), the most important application of optical mineralogy. In combination with geophysical and geochemical data and, of course, with field work, the immense body of results obtained by PLM has made it possible to reconstruct large-scale processes like e.g. volcanism, metamorphism and plate movements. In brief, without PLM work we would be missing essential information on how the Earth works.

PLM has been the most used method for the identification of minerals in rocks. Therefore, optical mineralogy has been an important component in geoscience education for more than a century.

### **Optical mineralogy and geoscience curricula**

Today, optical mineralogy is less applied in industry and at universities. Consequently, the knowledge base of mineral optics is dwindling. Optical mineralogy courses are beginning to disappear from geoscience curricula. At some departments, the subject has been reduced to a topic in the syllabus of mineralogy and petrology courses; at other departments, it is no longer taught at all.

This “decline of optical mineralogy” has been deplored and vividly debated on the MSA Talk list, and, e.g., in the *Journal of Geoscience Education* (Reinhardt, 2004) and in *Elements* (Kile, 2006; Ince 2006).

For geologists, the polarised light microscope is an analytical tool, not merely an instrument of magnification. No other instrument has allowed studying mineralogical and microstructural material properties at the same time. PLM is a classical and powerful method.

How then can optical mineralogy begin to disappear from the geoscience curricula? Two main factors are responsible:

Firstly, PLM is no longer the only method of studying minerals on the micro scale. (a) State-of-the-art scanning electron microscopes (SEM) allow both the identification of phases and the micro-structural characterization of solid materials. They do so down to the nanometer scale, which is inaccessible to optical microscopes. (b) At the same, the electron microprobe has - since decades - routinely been used for micro-chemical mineral analyses. Today, nobody with access to a microprobe would seriously consider determining plagioclase compositions from the optical measurement of axial angles. (c) Rietveld quantitative phase analysis from X-ray powder diffraction data is finding its way into petrography and will replace microscopic point counting.

The other factor is the curriculum. Science departments have to give their students the best possible professional education; their obligation is to acquaint them with new methods. Many of these are sophisticated instrumental methods like those mentioned above. Room has to be made for courses where these methods can be taught and practiced. So, partly, the dilemma is simply time. The overall duration of studies is fixed. This limits the number of courses. Old courses have to yield to new courses. Optical mineralogy is classical and has been taught for ages. This, in itself, makes it an “old” course, an endangered species.

### **Polarising microscopy vs. microbeam techniques**

In their uses, PLM and micro-beam techniques overlap. Micro-structural features and many of the mineral properties traditionally studied under the polarising microscope can conveniently be examined, as well, by SEM, and, at the same time, at resolutions down to the nanometer scale. Nonetheless, PLM remains a premier method for the study of rocks and minerals, particularly minerals in rocks. Micro-beam techniques supplant but do not replace PLM. In many cases, mineral investigations by SEM and microprobe are much facilitated by the previous examination of the sample by PLM, if they do not even require it.

With micro-beam techniques it is not possible to see the pleochroic colours of minerals and their interference colours and, thus, to make anisotropic properties of minerals visible. This is a shortcoming only partly compensated for by the possibility of in-situ chemical analyses.

### **Cost efficiency, ease of use, availability**

One main reason for the continued use of PLM is cost efficiency, ease of use, and availability. SEM and microprobe studies are excellent where studies ranging down to the micrometer and sub-micrometer scale are required and for micro-chemical analyses. However, they are comparatively expensive and time consuming, if they were to be used to determine the modal mineralogy in tens, if not hundreds, of thin sections from rock samples collected in the field.

It is much simpler to operate a light microscope – one has to switch it on and occasionally rotate the objective revolver - than to work with an SEM or even with an electron microprobe. With the polarised microscope (and a modest experience in rock microscopy), it is a matter of only minutes to identify the main minerals in a rock content and – simultaneously its microstructure. It is easy to distinguish between common polymorphs like calcite and aragonite or sillimanite and kyanite, which are hard to tell apart by microbeam techniques.

Polarising microscopes are comparatively cheap (excellent standard models are available from € 5000). They are portable. They do not require running expenses. They are much more generally available than SEMs and electron microprobes.

In order to just determine the modal mineralogy of a rock and its texture, the use of the SEM and/or the microprobe would be massive analytical overkill, inefficient and uneconomical. Here, PLM is still most useful and indispensable.

### **Searchable mineral optics databases**

A searchable database is likely to become available within the next few years cf. <<http://almandine.geol.wvu.edu/~dave/petsearch/>>. It will make use of existing databases like the IMA database <<http://rruff.info/ima/>>. Database programs greatly facilitate online identification of less common minerals by PLM. An excellent program was developed more than ten years ago by

Pedersen (1997). Its application is limited, because it is based on a very small number of minerals. But it does demonstrate the potential of this type of programs. They will make PLM attractive to a much wider group of users than and strengthen the application of optical mineralogy.

The advent of searchable databases for optical mineral identification are in themselves a strong argument in favour of an increased use of PLM and are likely to trigger a renaissance of this method, where it otherwise risks sinking into oblivion.

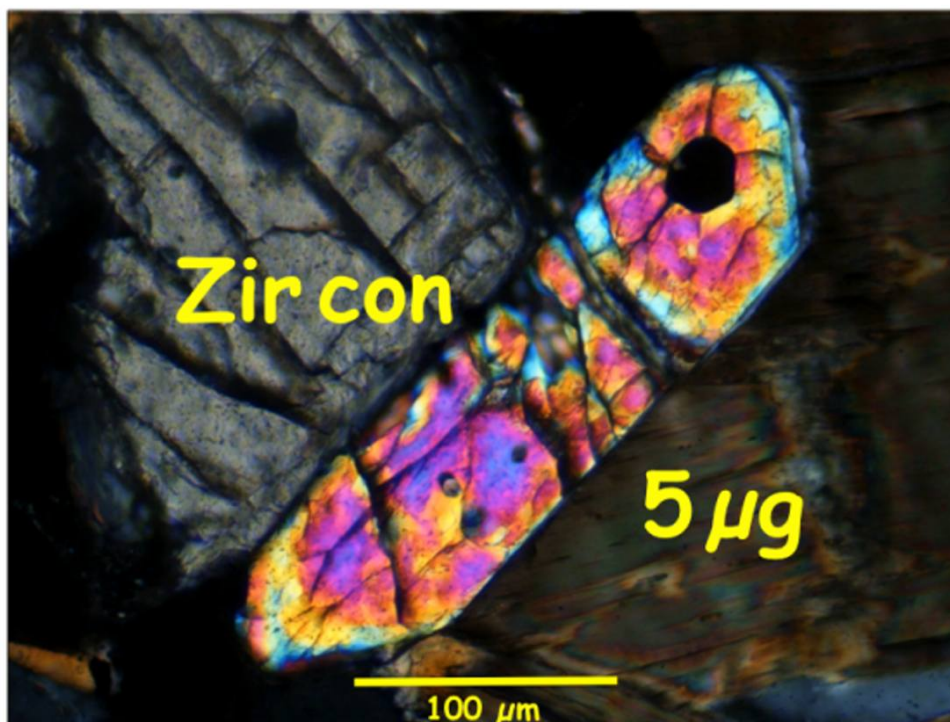


Figure 1. Zircon under crossed polars.

### **Advantages of PLM – a summary**

The advantages of the method can be summarized by four main points:

- non-destructive
- small amounts,  $\mu\text{g}$ -sized
- rapid identification
- cost-efficient

The method is *non-destructive* because it allows examination of minerals in-situ, in rock thin sections, where they can be studied in their natural textural configuration. Depending on the mineral

and grain size, safe determinations are possible of *amounts as small as a few micrograms* or even less. This is easy, e.g. with zircon (fig.1.), which, at the same time, allows a very *rapid identification*. To stay with this example, compared to any other method, PLM is not only the fastest method to determine this mineral, it is also the *most cost-efficient*.

## References

Ince, F., 2006. In Praise of Polarized Light Microscopy. Elements 2(5), 262

Kile, D., 2006. Polarized Light Microscopy in Geoscience Education: Relevant or Obsolete? Elements 2(4), 197 – 198

Pedersen, N., 1997. Polemic: a 32-bit windows program for the identification of minerals in thin section,. Computers & Geosciences, 23 (9), 1021-1026

Reinhardt, J., 2004. Optical Mineralogy in a Modern Earth Science Curriculum. J. Geoscience Education, 52 (1), 60 – 67.

## Teaching Optical Mineralogy: Practical Suggestions

Hans Dieter Zimmermann

*Dept. of Earth Sciences, Aarhus Universitet, DK-8000 Århus C (email: geolhans@geo.au.dk)*

### Introduction

Polarised light microscopy (PLM) is no longer the only method of studying minerals on the micro-scale and there is not much room in modern geoscience curricula for extended optical mineralogy teaching. (Zimmermann, 2010). Nonetheless, the polarising microscope remains a premier tool for the study of solid lithosphere materials. The question is less whether to keep optical mineralogy as part the geo-science education or not, but how to teach it despite the imposing constraints.

At the Dept. of Earth Sciences at Aarhus University (Denmark), we have, for more than 20 years, been teaching a second-year compact course on Polarised Light Microscopy, renamed Rock Microscopy in later years (table 1). The course has turned out to be quite popular with the students.

With the experience from this course, I would like to present some suggestions for teaching optical mineralogy. They concern (1) simple means to help a basic understanding of *crystal optics*, (2) the optical description of minerals and their *systematic identification*, (3) *practical work* and, finally, a reference to a (4) *crystallisation experiment*.

Table 1

Teaching period:	7 weeks, 50 hours
Lectures:	18 hours,
Practical:	32 hours
Compulsory programme:	
-	Bi-weekly assignments (description of rock thin sections)
-	Group research project
Credit points:	5 ECTS
Level:	2 <sup>nd</sup> year

## 1. Crystal optics

Proficient use of PLM requires a solid grasp on the relation between crystal structures, crystal chemistry and optical properties, in short, on crystal optics. Yet, this topic is the crux of many an optical mineralogy course and prone to turn students away.

The most important phenomenon of crystal optics is double-refraction. Its principal features are easily imparted by hands-on experiments using the following:

- calcite rhomb (edge lengths  $\geq 25\text{mm}$ ),
- quartz crystal with hexagonal prism (length  $\geq 40\text{ mm}$ , diameter  $\geq 20\text{ mm}$ ),
- muscovite sheet ( $\geq 30\text{ mm} \times \geq 30\text{ mm}$ , thickness to yield 2<sup>nd</sup> – 4<sup>th</sup> order interference colours)
- two polarising filters (50mm x 50mm).

We hand each student a personal set of these materials to keep.

### (a) Double-refraction

The calcite specimen is placed on a piece of paper (paper and rhombohedral face are parallel) and a dot, or some other object on the paper, is viewed through the calcite rhomb. Two images are observed. Rotation of the rhomb around an axis normal to the paper plane shows, that one image stays fixed, whilst the other follows a circle.

This corresponds to the ordinary and extraordinary ray, respectively. The observation is classical. It was first described by the great Danish renaissance scholar Rasmus Bartholin (1669). He is the scientific discoverer of double-refraction.

A polarising filter placed on top of the upper rhombohedral face of the calcite crystals allows additional crystal optical observations: Rotating the polarizing filter around the axis normal to the rhomb face reveals that the light passing through the crystal is plane-polarised in two directions and that these directions are perpendicular to each other. Using a (water-soluble) felt-pen, and plotting these directions on the crystal faces, it immediately becomes obvious that light in the crystal is plane-polarised parallel with and perpendicular to – the c-axis (Fig. 1 A, B). Furthermore, it shows that the vibration direction of the extraordinary ray is parallel with the crystallographic c-axis, and

that the ordinary direction is perpendicular to it. This is fundamental and applies to the group of all “gonal” crystals (trigonal, tetragonal, hexagonal).

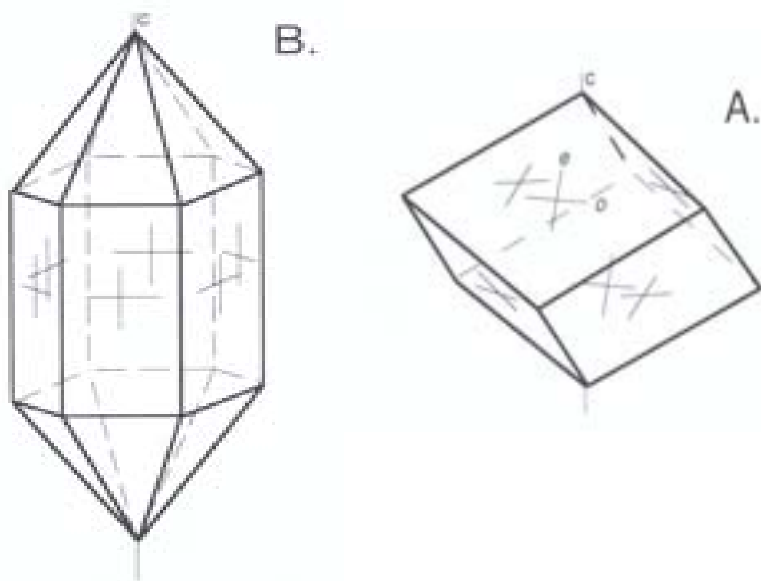


Figure 1. Vibration directions plotted on crystal faces: (A) calcite rhombohedron, (B) a quartz prism.

Repetition of the experiment with quartz prisms confirms the existence of two, mutually perpendicular, vibration directions: one parallel with the c-axis and the other perpendicular to it.

In thin plates viewed in transmitted light and between crossed polars, double-refraction manifests itself in interference colours. This is easily demonstrated using thin cleavage sheets of muscovite.

For detailed descriptions of these hands-on lab experiments, see Zimmermann (1997). - With sufficiently big calcite rhombs and quartz crystals, and with large polarizing sheets, these experiments are well suited for lecture demonstrations using an overhead projector.

Where a sufficiently large (edge length > 50mm) and very clear calcite rhomb is available, it is possible to give a – fairly spectacular – lecture demonstration of double-refraction by shining an unpolarised laser beam through the crystal and showing that one ray goes in and two come out. For details of this experiment and the one below, cf. also Zimmermann (1997).



### (b) Interference figures

Interference figures are much decried as a crystal optical phenomenon, difficult to observe and hard to interpret. Usually, they are viewed in the polarizing microscope. Also, here, it may help to demystify crystal optics some and to show that interference figures can be observed quite simply and that they do not necessarily require a microscope. Interference figures are not images of the object but an interference pattern, which becomes visible when the anisotropic crystal is placed between crossed polars and viewed against the light in such a way that the rays passing through the crystal form a large cone with a wide angular aperture (Fig. 2).

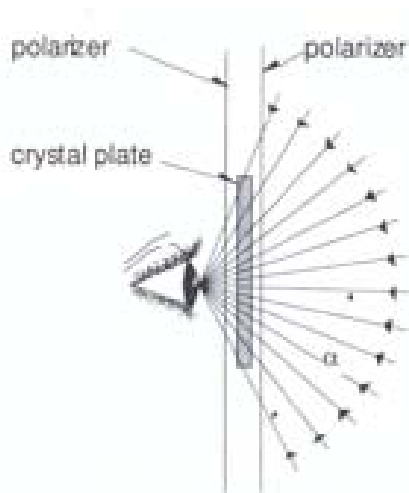


Figure 2. Macroscopic observation of interference figures

All you need is a transparent mineral, e.g. a muscovite sheet, and two polarisers. The muscovite sheet is sandwiched between crossed polars, held against a light source and brought as closely to the eye as possible. You will then see an interference figure.

### (c) Double-refraction and crystal structure

Interference colours are an expression of the double-refraction. The extent of the double refractions reflects the degree of optical anisotropy, which, again, is controlled by the crystal structure. This correlation can also be demonstrated in a rather simple way: Place a plastic film (e.g. from a transparent plastic bag) between crossed polars, view it against a light source and stretch it slowly.

To begin with, in the unstretched state, it will show no – or only very low - interference colours: the chain-like polyethylene molecules it consists of do not originally make up a long-range order.

However, the more the plastic material is stretched, the more the molecular chains are forced into a quasi-parallel alignment and thus a long-range order is imposed mechanically and interference colours of increasing order are observed. This long-range order of the polyethylene molecules could be seen as analog to solid chain-silicates, which are polymer crystals.

The experiments above are to make it easier for the student to understand the anisotropic phenomena seen in the polarizing microscope and to show that vibration directions are fixed by the crystal structure and that, therefore, the optical indicatrix can be understood as firmly anchored to the crystal.

## **2. Systematic identification**

A main objective with optical mineralogy courses is to give the students enough practice with the microscopy of minerals so that they easily can recognize common minerals. The traditional teaching approach is to first present the most important rock-forming minerals, mineral by mineral. Then, to pass on to the microscopy of rocks.

In our optical mineralogy course, we have chosen a more inductive approach. The introductory sections deal with the optical, crystal-optical and instrumental basis for polarising microscopic examinations. They are followed by three chapters:

(a) Observations in plane-polarised light, (b) Observations with crossed polars, interference colours, and, (c) Conoscopy, observation of interference figures. Together, all sections above provide the necessary background for PLM. All are accompanied by practical exercises.

Then, we give an introduction to the systematics of mineral description and determination and proceed immediately to the identification of minerals in rocks without previous mineral by mineral presentations. As help for the systematic determinations, we use work sheets: One for recording all observations on a given mineral (Fig. 3) and another for its identification by systematic search (Fig. 4). Search criteria are the mineral properties observed.

The important point is to begin the search with the most selective, the most exclusive, property. Suppose a mineral is described – amongst others – as colourless, biaxially negative and with a birefringence of  $\Delta n \approx 0.40$  and an optic angle of  $2V \approx 35^\circ \pm 5^\circ$ . Then “colourless” and “biaxially

negative” would not be useful as search criteria because most minerals appear colourless under the microscope and the majority of all minerals are biaxially negative. However, both the fairly high birefringence of  $\Delta n \approx 0.40$ , and an optic angle  $2V$  of  $30^\circ$  to  $40^\circ$  are valuable criteria. Each of these two properties is restricted to a small number of minerals. In combination, they are very specific. - The more selective the first criteria, the more efficient the search. Efficient searches converge quickly.

The approach is illustrated by the two work sheets (Figs. 3 & 4). The systematic search requires using determinative tables, i.e. tables which, for each single mineral optic property, list all the minerals showing this very property. Many optical mineralogy textbooks contain such tables and, thus, can serve as search manuals, see e.g., Kerr, 1977 (still one of the best, though over 30 years old) and Nesse, 2004 (hardback), 2009 (paperback).

These two texts - like most other optical mineralogy books - consider some 100 - 200 different minerals. This is much in excess of the number of common rock-forming minerals (15 - 20). Even, when adding the metamorphic index minerals and frequent accessory minerals, there are hardly more than 30 – 35 minerals to take into account with most rocks. In the first run, we limit the search to these 35 minerals. This allows for a fairly quick search with a good success rate.

To begin, each mineral is an unknown mineral the students must identify. Thereby, they discover the typical features of different minerals.

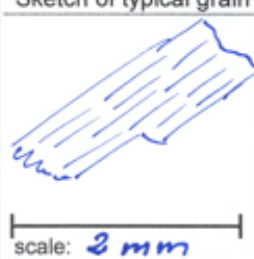



The result for each mineral identification is checked. This is what the last part of the second work sheet refers to (Fig. 4): One’s own description of the mineral identified is compared to that in mineral optics book or on the web, e.g. <http://webmineral.com/>. If there is agreement, the mineral is taken as determined correctly. Otherwise, mineral description and search are revised.

Once, searchable databases are available, mineral identification will become faster, see, e.g., <http://almandine.geol.wvu.edu/~dave/petsearch/>.

specimen # /thin section # **I** Mineral: **C**  
**GT3**

## Optical mineral determination

### 1. Examination and description

Mineral appears	opaque	translucent	<b>transparent</b>
Typical crystal shape, contour	anhedral	<b>subhedral</b>	euhedral
→ Typical grain shape, habitus	equidimensional	<b>elongate</b>	prismatic columnar acicular fibrous skeletal   Other:
⇒ Colour/s	<b>none</b> (= colourless)	grey	violet blue green
Colour intensity	<b>none</b>	weak	medium strong
Pleochroism	<b>none</b>	weak	medium strong
→ Cleavage traces and quality	no cleavage traces observed	1. cleavage direction: poor distinct	2. cleavage direction: <b>perfect</b> poor distinct perfect
⇒ Relief	weak	<b>moderate</b>	strong very strong
⇒ Relative RI (Becke line)	< 1,54	≈ 1,54	<b>&gt; 1,54</b>
Grain size, relative	small	<b>medium</b>	large
Grain size, absolute	<b>2 mm</b>		
Amount in vol %	<b>5</b>		
⇒ Optic mode	isotropic	<b>anisotropic</b>	
Max. interference colour	masked	grey red	white violet <b>blue</b> <b>orange</b> <b>green</b>
Interference colour order	I	II	<b>III</b> >III
⇒ Δn <sub>max</sub> ≈	<b>0.040</b>		
Extinction/direction of reference	no dir. of ref.	<b>parallel</b>	oblique wrt. cleavage/s <b>edge/s</b>
→ Twins	<b>none observed</b>	simple	polysynthetic   other:
⇒ Axiality	not determined	uniaxial	<b>biaxial</b>
⇒ Optic sign	not determined	pos. neg.	pos. neutral <b>neg.</b>
⇒ Axial angle 2V	not determined	2V ≈ <b>30°-40°</b>	
Sketch of typical grain	Axis figure sketches		
	<div style="display: flex; justify-content: space-around;"> <div style="text-align: center;"> <p>Parallel position</p>  </div> <div style="text-align: center;"> <p>45° position</p>  </div> </div>		
Location of Grains examined			

Additional observations, special properties (angle between cleavage directions, fractures, inclusions, alteration, sign of elongation, zoning, angle of extinction etc.):

Figure 3. Worksheet: Mineral description

specimen #, thin section #

GT 3

Mineral: C

## 2. IDENTIFICATION

- systematic search -

SEARCH STEP	1.	2.	3.	4.
SEARCH CRITERIA, DISTINCTIVE PROPERTIES	$\Delta n = 0.040$	$2V = 30^\circ - 40^\circ$		
REFERENCE Determinative tables used. Page # and tab.#, fig.# etc	NESSE (2004) Fig. 81, p. 320-322	NESSE Fig. 81		
MINERALS (1. column: mineral names, following columns: tick mark)	CUMINGTONITE			
	AEGIRINE-AUGITE			
	OLIVINE			
	EPIDOTE			
	AEGIRINE			
	MUSCOVITE	✓		
	BIOTITE			
RESULT OF SEARCH	MUSCOVITE			

## 3. CONTROL

- verification -

REFERENCE/S for mineral description	NESSE (2004), p. 169 KERR (1977), p. 385
DIAGNOSTIC PROPERTIES*)	colourless, $\Delta n \approx 0.40$ , $2V \approx 40^\circ$ , opt. negative, one perfect cleavage trace, extinction parallel with cleavage
MINERAL DETERMINED AS:	MUSCOVITE

\*) Enter, here, both the distinctive properties used as search criteria in the systematic search above and additional characteristic properties like angle between cleavage directions, sign of elongation etc (see also front page, bottom)

Figure 4. Worksheet: Mineral identification

### **3. Practical work**

In our mineral optics course, emphasis is on practical work. All theory and the lab sessions dealing with the principal aspects of crystal optics and of PLM are concentrated within the first third of the lessons. The remaining two thirds of the time are fully dedicated to microscopy work.

#### **(a) Lab work**

Students examine and describe thin sections of at least twelve different rocks and hand in two descriptions every week. These are corrected in detail, and returned within 48 hours. The brief turn-around ensures a quick feedback, thereby strengthening the learning effect.

In addition to the equipment (good polarising microscopes), the quality of the sample material is decisive for the success of the practical teaching. The rock samples we use are carefully selected to be representative of common rocks and to be relatively fresh, i.e. preferably the minerals are not altered, or, at least, as little as possible. All rocks studied in the course exist as class sets in form of both small hand-specimens and thin sections. This way, all students can work with the same rock at the same time.

In the beginning of each lab session, the students' own descriptions of the rock studied during the previous session are returned with corrections and comments. The students are also given a model description of the rock. Then, the minerals in the rock and its microstructure are projected on to the screen "live", i.e. directly from the microscope and all essential features of the rock are discussed in view of these projections.

Our microscopy lab is equipped with 14 polarising microscopes. However, we try to limit group sizes to 8 to 10 participants. During each lab session, usually, two instructors are present to help students with the microscopy work. Thus, students receive an intensive training and acquire practice.

#### **(b) Research project**

An additional part of the practical work is a little research project the students are given towards the end of the course. They work in groups of two or three. The project's objective is to familiarise the



students with all steps of rock examination: selection of suitable specimens, preparation of samples, PLM investigations, and final report on the results.

Each group prepares its own rock samples (cutting and sawing them) and hands in a slab of each sample to the thin section lab. Preparation of the thin sections is left to experienced lab technicians but the students observe and follow all steps of the process.

At the beginning of the microscopy work, thin sections are scanned with a high resolution both in plane-polarised light and under crossed polars. This way, good overviews of thin section can be obtained. An ordinary scanner is perfectly suited for this purpose.

During microscopy, frequent photomicrographs are taken. Both the scanned images and the micrographs are used in the report to illustrate minerals and textures.

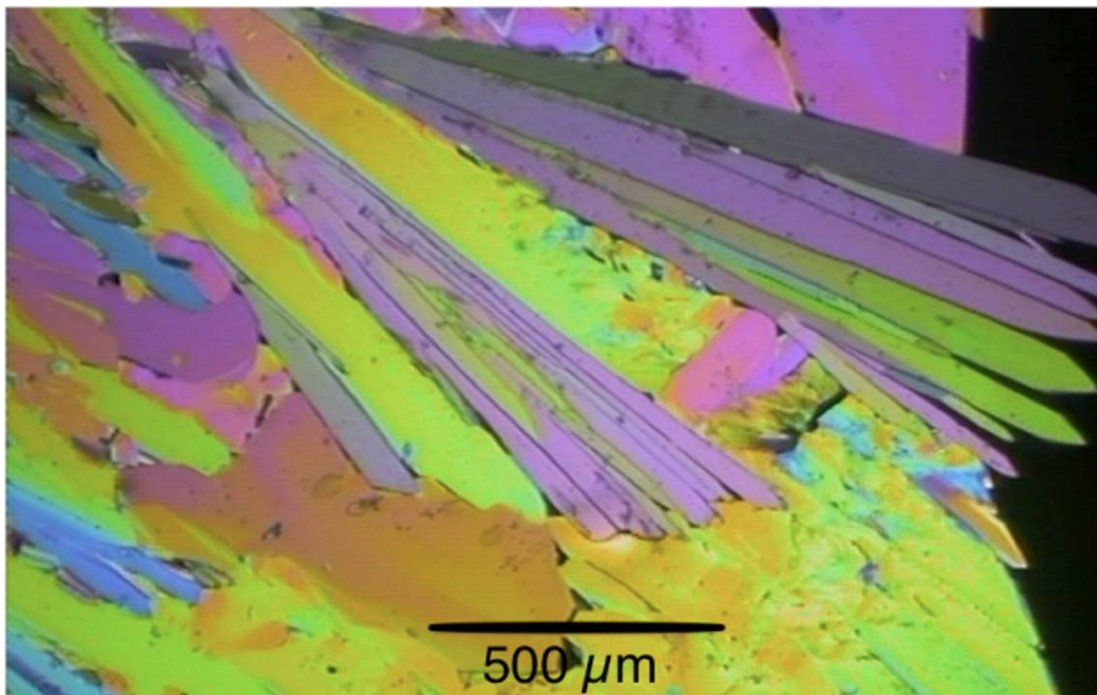


Figure 5. Crystallisation experiment with salol. Crossed polars. The black area, in the part of the image, represents melt.

#### **4. Crystallisation experiment**

Crystals (if non-cubic) are anisotropic and thus birefringent, liquids are not. This implies a dramatic change in the optical properties of a material crystallising from a melt. With igneous rocks, observation of this change under the polarizing microscope is not realistic; the liquidus temperatures are too high. For a basaltic composition, for instance, they are at 1200 C.

This problem can be remedied by using low-melting substances and a suitable heating stage. An appropriate low-melting compound is salol (phenyl salicylate). It melts at 42 C. The salol experiment is a classical experiment to demonstrate crystal growth (cf. e.g. <http://www.geolsoc.org.uk/gsl/education/resources/rockcycle/page3656.html>). It yields spectacular images, when observed under crossed polars (Krämer, 1979). It allows, at the same time, to demonstrate the relation between magmatic textures (grain size) and cooling rate.

#### **Acknowledgement**

The author gratefully acknowledges travel support by the Nordic Mineralogical Network to this year's meeting in Tallinn. A great thanks to Jüri Nemliher for his invitation to Estonia and for the excellent arrangement of the most pleasant and very inspiring meeting at the Tallinn University of Technology and for the two impressive excursions he guided. - As this year's conference marks the transition to a new stage of the Nordic Mineralogical Network, I take this opportunity to address many thanks to Tonci Balic-Zunic for his initiative of having founded the Network and for all the work he – throughout the years - has put into this very successful enterprise.

#### **Note**

Worksheets (cf. Figs. 3 & 4) and an – unedited - video of the crystallisation experiment with salol can be obtained from [geolhans@geo.au.dk](mailto:geolhans@geo.au.dk).



## References

Bartholin, Rasmus. Experimenta crystalli islandici disdiacastici quibus mira & insolita refractio detegitur. Hafniae, 1669. English translation: Experiments with the double refracting Iceland crystal which led to the discovery of a marvelous and strange refraction, tr. by Werner Brandt. Westtown, Pa., 1959.

Kerr, R.F., Optical Mineralogy, 4<sup>th</sup> ed., McGraw Hill, New York, 1977, 492 p.

Krämer, E., 1979, Faszination durch Phasenübergänge. Contact (Zeitschrift für die Freunde des Hauses Leybold-Heraeus), Nr. 21, March 1979, 19 – 21

Nesse, W.D., Introduction to Optical Mineralogy, 3<sup>rd</sup> ed., Oxford University Press, 2004, 348 p.

Nesse, W.D., Introduction to Optical Mineralogy (Paperback edition), Oxford University Press. 2009, 464 p.

Zimmermann, H.D., 1997. Experiments in Crystal Optics, in: Brady, JB et al (eds), Teaching Mineralogy, Mineralogical Society of America, Washington, D.C., 297 – 308

Zimmermann, H.D., 2010. Optical Mineralogy – An Anachronism? This volume.

## **Experimental study on carbon dioxide contents in basanitic and leucititic melts**

Hans Dieter Zimmermann<sup>1</sup> and John R. Holloway<sup>2</sup>

1) *Dept. of Earth Sciences, Aarhus Universitet, DK-8000 Århus C (email: geolhans@geo.au.dk)*

2) *Dept. of Geological Sciences and Dept. of Chemistry and Biochemistry, Arizona State University, Tempe, AZ 85827, USA*

### **Introduction**

CO<sub>2</sub> is the second most abundant volatile discharged from the solid Earth. Most of it comes from igneous sources. Data on magmatic CO<sub>2</sub> concentrations are needed to model the global carbon cycle and in connection with topics such as volcanic gas emissions, greenhouse effect, eruption mechanisms.

It is difficult to quantify the annual subaerial CO<sub>2</sub> fluxes into the atmosphere (Shinohara, H., 2008; Kerrick, 2001). Estimates are primarily obtained from airborne and ground based remote spectroscopy methods to measure volcanic gas emission rates. Such measurements are available only for a limited number of active volcanoes. They cannot be used directly to constrain the CO<sub>2</sub> discharge from igneous sources. Assessing flux rates requires working with assumptions and large extrapolations. Uncertainties in the range of, at least, ±50% are realistic (Jambon, 1994). According to Kerrick (2001) “the best approximation of the total contemporary CO<sub>2</sub> flux from subaerial volcanic degassing is  $\sim 2.0 - 2.5 \times 10^{12}$  mol/y  $10^{12}$  mol/yr.” This corresponds to  $\sim 88 - 110 \times 10^6$  tons CO<sub>2</sub>/yr and represents roughly 0.5% of the annual anthropogenic CO<sub>2</sub> emission ( $\sim 27$  Gt).

Remote measurements do not allow correlating CO<sub>2</sub> emission rates and melt chemistry. The example of Mount Etna shows, however, that this is a question of great principal interest. Especially, since Mount Etna together with Popocatépetl, is the volcano with the highest subaerial CO<sub>2</sub> emission. The compositions of the Etna pyroclastics have evolved from tholeiitic to alkaline and the CO<sub>2</sub> discharge rates have varied.

Experimental studies on volatile solubilities in magmatic melts supplement data on volatile emission rates and provide upper limits for volatile contents in magmas.

CO<sub>2</sub> contents in silicate melts are controlled by pressure, temperature, oxygen fugacity and melt chemistry. For common melts, the effects of P, T, and  $f(\text{O}_2)$  have been fairly well constrained by previous investigations. However, no-self consistent data set exists on the variation of the CO<sub>2</sub>-solubility with melt composition. Earlier investigations suggest that pre-eruptive CO<sub>2</sub> contents in leucitite melts are two to three times higher than in basanite melts. Therefore, the system basanite - leucitite appears particularly suited for experimentally quantifying the dependence of CO<sub>2</sub> solubility on melt chemistry.

### Starting materials

Five melt compositions were synthesized. They represent a pseudo-binary series with basanite, B100, and (a Ca-rich) leucitite, L100, as end-members (table 1) and with B75L25, B50L50 and B25L75 as intermediate compositions. The starting

	BASANITE B100		LEUCITITE L100	
	weight%	mole%	weight%	mole%
SiO <sub>2</sub>	45	50	44	47
TiO <sub>2</sub>	2.9	2.4	2.7	2.1
Al <sub>2</sub> O <sub>3</sub>	15	9.6	12	8
Fe <sub>2</sub> O <sub>3</sub>	3.8	1.6	3.2	1.3
FeO	9.2	8.3	6.2	5.5
MgO	8.3	13	9.2	14
CaO	8.2	9.5	14	16
Na <sub>2</sub> O	4.4	4.6	3.2	3.3
K <sub>2</sub> O	1.2	0.8	3.6	2.3
P <sub>2</sub> O <sub>5</sub>	0.8	0.4	0.8	0.3

Table 1. Composition of starting materials.

materials were produced in two steps: (1) From an oxide mix of all components apart from iron and apart from the alkalis and some of the calcium, a glass was prepared and then ground. (2) The remaining components were added as powder mix consisting of Fe<sub>2</sub>O<sub>3</sub>, FeO, Na<sub>2</sub>CO<sub>3</sub>, K<sub>2</sub>CO<sub>3</sub> and Ca<sub>2</sub>CO<sub>3</sub>.

The carbonates acted as carbon sources in the starting material, providing initial CO<sub>2</sub> contents of 7.3 to 8.7 weight percents. To assure oxidizing conditions during runs, we adjusted the Fe<sub>2</sub>O<sub>3</sub>/FeO ratios to yield an oxygen fugacity of 1.0 log unit above the Ni-NiO buffer.

### **Experimental techniques and run conditions**

All experiments were carried out in non-end loaded piston-cylinder apparatuses and conducted at 1.5 GPa, and at temperatures of 1500°C and 1400°C, respectively. In the 1500°C runs, we used Fe-doped platinum capsules, and in the 1400°C runs, palladium-gold capsules (Pd<sub>25</sub>Au<sub>75</sub>). All capsules were welded shut and leak tested prior to the runs. Depending on temperature, the runs lasted between 40 and 150 minutes and were terminated by isobaric quenching. At the beginning of each experiment, the run pressure was applied first and was kept constant during heating up to run temperature. By quenching, melts were preserved as glasses. Each starting mix had an excess of CO<sub>2</sub>. Consequently, quench glasses from the runs contain bubbles, if the capsule remained sealed. Bubbles in run products are, therefore, the criterion for capsule tightness and for CO<sub>2</sub>-saturation of the melt.

### **Analysis**

Composition and homogeneity of all run products were examined with the electron microprobe. Melts contained in platinum capsules, had lost, during the runs, between 3 to 15%, relative, of their initial Fe<sub>2</sub>O<sub>3</sub> contents. The Fe was lost to the Pt-capsules despite pre-saturation with iron. - CO<sub>2</sub> contents in the run product glasses were analysed by Secondary Ion Mass Spectroscopy on a Cameca IMS 3f, using a primary ion beam of mass filtered <sup>16</sup>O<sup>-</sup> with a spot diameter of 15 – 25 μm. Of each sample, we analysed two to five spots. The speciation was determined by FTIR micro-reflectance measurements. They show carbon in the quenched melts to be dissolved as CO<sub>2</sub><sup>3-</sup> (Grzechnik et al, 1996).

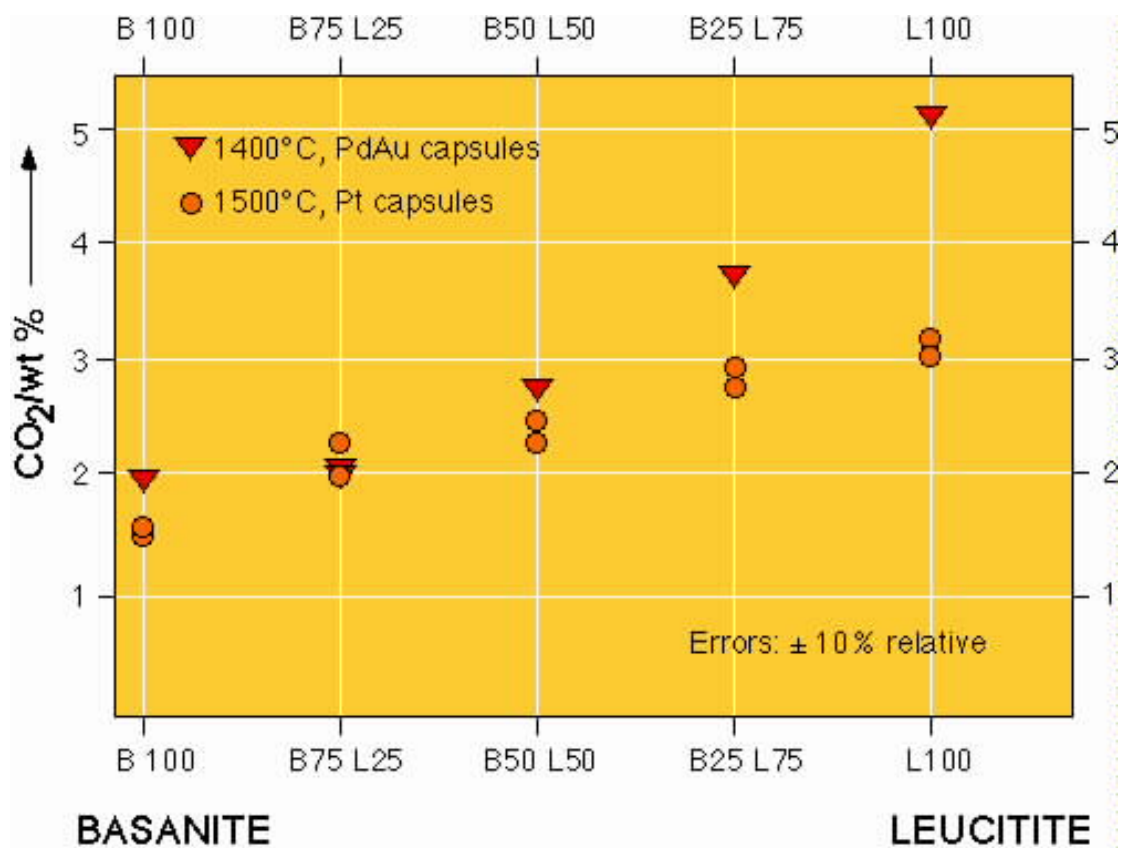


Figure 2. CO<sub>2</sub> solubilities in basanitic to leucitic melts at 1.5 GPa, and at 1400°C and 1500°C.

## Results

At 1500°C and 1.5GPa, CO<sub>2</sub> solubilities range from 1.5 weight% in basanite over 2.5 wt% for the basanite50-leucitite50 (B50L50) composition to 3.2wt% in leucitite. At 1400°C, basanite dissolves 1.9 wt% CO<sub>2</sub>, B50L50 2.8 wt% and leucitite 5.2 wt%. The analytical error is ca. ± 10 %, relative. Altogether, we have determined 16 new solubility-composition points. Our results agree with earlier data on the CO<sub>2</sub> solubilities in basanite and leucitite melts (see e.g. Thibault & Holloway, 1994; Holloway & Blank, 1994). They suggest that CO<sub>2</sub> concentrations in the melts correlate positively with increasing Ca/(Ca+Mg) and increasing non-bridging oxygens (NBO/T). The solubility trend between basanite and leucitite appears smooth (Fig. 1). The data set at 1400°C shows a small, but significant, deviation from linearity across the pseudo-binary join.

## References

Grzechnik, A., Zimmermann, H.D., King, P.L., McMillan, P.F. and Hervig, R.L., 1996. FTIR micro-reflectance measurements of the  $\text{CO}_3^{2-}$  ion content in basaltic and leucitic glasses. *Contrib.Mineral.Petrol.*, 125 (4), 311-318

Holloway, J.R. and Blank J.G., 1994. Applications of experimental results to C-O-H species in natural melts. In: M.R.Carroll & J.R.Holloway (eds), *Volatiles in Magmas, Reviews in Mineralogy* 10, 187-230

Jambon, A., 1994. Earth degassing and large-scale geochemical cycling of volatile elements. *Rev. Mineral. Geochem.* 30;1; p. 479-517

Kerrick, D.M., 2001. Present and past nonanthropogenic  $\text{CO}_2$  degassing from the solid Earth. *Rev. Geophys.* 39 (4), 565 – 585.

Shinohara, H., 2008. Excess degassing from volcanoes and its role on eruptive and intrusive activity. *Rev. Geophys.*, 46, 31p

Thibault Y. and Holloway J.R., 1994. Solubility of  $\text{CO}_2$  in a Ca-rich leucitite: effects of pressure, temperature and oxygen fugacity. *Contrib. Mineral. Petrol.* 116, 216-224